Research Square

Preprints are preliminary reports that have not undergone peer review.
They should not be considered conclusive, used to inform clinical practice,
or referenced by the media as validated information.

Tau PET in tauopathies: a systematic review and meta-analysis of regional tau deposition and diagnostic performance

Quanling Jiang
University Hospital of Bern
Jing Wang
Huashan Hospital
Jingjie Ge
Huashan Hospital
Jiaying Lu
Huashan Hospital
Huamei Lin
Huashan Hospital
Yang Liu
Huashan Hospital
Axel Rominger
University of Bern
Chuantao Zuo
Huashan Hospital
Ruiqing Ni
ruiqing.ni@unibe.ch
University of Bern

Systematic Review

Keywords: Tau PET, Tauopathies, Diagnostic accuracy, Regional tau uptake patterns, Meta-analysis

Posted Date: November 19th, 2026

DOI: https://doi.org/10.21203/rs.3.rs-11552225/v1

License: This work is licensed under a Creative Commons Attribution 4.0 International License. Read Full License

Additional Declarations: No competing interests reported.

Abstract

Background

Tauopathies represent a diverse group of neurodegenerative diseases characterized by abnormal tau protein aggregation. Accurate differential diagnosis remains challenging due to overlapping clinical features and the limited specificity of conventional imaging. Tau positron emission tomography (PET) imaging represents a promising diagnostic tool for tauopathies. This systematic review and meta-analysis aimed to examine regional uptake patterns and assess the diagnostic performance of tau PET across major tauopathies.

Methods

A systematic review and meta-analysis were conducted to evaluate regional tau deposition and the diagnostic performance of tau PET. Regional tau tracer uptake values and diagnostic accuracy parameters (sensitivity, specificity, and area under the curve [AUC]) were analyzed using random effects models to estimate standardized mean differences (SMD) and pooled diagnostic performance, respectively.

Results

Compared with HCs, patients with Alzheimer's disease (AD) had significantly elevated tau uptake in 27 brain regions (SMD range: 0.39–2.58; $p < 0.01$), patients with progressive supranuclear palsy (PSP) in eight regions (0.41–1.71; $p < 0.05$), and patients with corticobasal syndrome (CBS) in four regions (1.06–1.86; $p < 0.01$). The pooled AUCs for distinguishing AD, PSP, and AD/mild cognitive impairment (MCI) patients from HCs were 0.92 (95% CI: 0.89–0.96), 0.92 (0.85–0.99), and 0.84 (0.74–0.94), respectively. Subgroup analyses revealed differences in tau uptake and diagnostic accuracy by outcome type, atlas application, tracer type, and generation.

Conclusions

Our findings demonstrate that tau PET reveals disease-specific uptake patterns with high diagnostic accuracy across tauopathies. The distinct spatial distributions of AD, PSP, and CBS provide valuable neuroimaging signatures for differential diagnosis. These results support the use of tau PET as a promising clinical biomarker, although methodological standardization is essential for optimal implementation.

Introduction

Tau, a microtubule-associated protein essential for axonal integrity, plays a crucial role in multiple neurodegenerative disorders, collectively known as tauopathies [1]. Pathological hyperphosphorylation triggers microtubule detachment and prion-like propagation of tau aggregates through neural circuits [2]. These disorders are characterized by the abnormal aggregation of tau protein and can be classified based on their predominant tau isoforms: 3-repeat (3R), 4-repeat (4R) variants, or mixed 3R/4R variants. Alzheimer's disease (AD) features mixed 3R/4R tau deposits, while progressive supranuclear palsy (PSP) and corticobasal degeneration (CBD) are characterized by 4R tau pathology [3].

Accurate antemortem diagnosis of tauopathies remains a significant clinical challenge because of substantial phenotypic overlap. For instance, corticobasal syndrome (CBS) can be caused by various underlying pathologies, with only 32% of patients showing CBD pathology at autopsy, while 31% of patients harbor PSP and 20% show AD pathology [4]. This diagnostic uncertainty has important therapeutic implications, as treatment approaches differ significantly between tauopathies [5]. Misdiagnosis can lead to ineffective interventions and compromise clinical trial outcomes [6, 7],

highlighting the urgent need for more accurate diagnostic tools, particularly as tau-targeted therapies enter clinical trials [8–10].

Positron emission tomography (PET) with tau-specific tracers has emerged as a promising approach for in vivo visualization of tau pathology [11]. First-generation tau PET tracers such as [^{18}F]AV-1451, the THK series, and [^{11}C]PBB3 demonstrated utility in AD but showed limitations, including off-target binding [12]. Second-generation tracers (including [^{18}F]PI-2620, [^{18}F]PM-PBB3, [^{18}F]MK-6240, [^{18}F]RO-948, and [^{18}F]GTP1) have been developed with improved specificity [13, 14]. Despite these advances, the clinical translation of tau PET faces several challenges, including inconsistent topographic patterns across studies and variability in diagnostic accuracy between tracers. For example, contradictory findings regarding midbrain tau signals in PSP have been reported with different tracers, complicating interpretation [15, 16].

To date, no comprehensive meta-analysis has addressed two fundamental questions: (1) whether disease-specific tau topographic signatures exist across major tauopathies and (2) how tracer type and methodology influence diagnostic accuracy. Addressing these questions is essential for establishing tau PET as a reliable biomarker for clinical use and therapeutic development.

Here, we present the first PRISMA-compliant meta-analysis integrating 80 studies (n = 9,166) to (1) map syndrome-specific tau deposition patterns across AD, PSP, and CBS; (2) quantify the diagnostic accuracy of current tau PET tracers in AD, PSP, and AD/mild cognitive impairment (MCI); and (3) evaluate the impact of methodological factors on these measures. Our findings establish tau PET as a promising tool for tauopathy diagnosis while identifying standardization requirements for its optimal clinical application.

Methods

Study Design and Registration

We conducted this PRISMA-compliant systematic review and meta-analysis (prospective PROSPERO registration: CRD42024609011) to ensure transparent reporting of search strategies, study selection, and data synthesis. Ethics committee approval was waived, as this study synthesized existing published data without direct human subject involvement.

Search strategy

Two investigators independently searched Ovid MEDLINE, Embase, and the Web of Science Core Collection until July 27, 2024, using a predefined Boolean syntax combining (1) tau tracer names ([^{18}F]AV-1451, [^{18}F]MK-6240, etc.), (2) PET imaging terms, (3) tauopathy diagnoses (AD, PSP, CBS), and (4) diagnostic accuracy metrics (sensitivity [SE], specificity [SP]). We excluded non-English articles, studies lacking quantitative region-level tau PET data, and articles without diagnostic data. The full search strings are provided in Supplementary Methods 1.

Eligibility criteria and study selection

Two blinded reviewers independently screened titles and abstracts, resolving conflicts with a third reviewer. The included studies met the inclusion and exclusion criteria, which are detailed in Supplementary Methods 2.

Data extraction

Two investigators independently extracted data from all the studies that met the inclusion criteria. Data collection included study characteristics (author's first name, publication date, type of tau tracer, and study design), subject characteristics (sample size, disease entities, age, and percentage of females), data characteristics, and data processing methods (atlas for brain region division, outcome measures for tau burden, and reference brain regions). The primary outcomes included tau tracer uptake values for each group (see Supplementary Material 2) and diagnostic accuracy metrics (sensitivity, specificity, area under the curve [AUC], true positives [TP], false positives [FP], true negatives [TN], and false negatives [FN]), which are presented in contingency tables (Supplementary Tables 2–4). The highest performance from each study was selected based on the AUC.

Quality assessment

The quality of the included studies was assessed using the Quality Assessment of Diagnostic Accuracy Studies-2 (QUADAS-2) [17] and/or the Newcastle–Ottawa Scale (NOS) [18]. If tau PET data across brain regions were extracted from the studies, the NOS was applied for assessment. Similarly, if the classification performance of tau PET was extracted, QUADAS-2 was used for evaluation. A comprehensive list of the questions used to evaluate research quality can be found in Supplementary Tables 7–8. All the studies were reviewed and analyzed by a minimum of two independent authors. Any disagreements were resolved through consensus or by involving a third reviewer. Stata software (v. 18.0) was used to assess the methodological quality of the included studies. The detailed assessment results are shown in a diagram in Supplementary Tables 5–6 and Supplementary Figs. 19–20. Visual inspection of funnel plot asymmetry and Egger's regression test were employed to assess publication bias (see Supplementary Figs. 21–27).

Statistical analysis

All data analyses were performed using the meta package (v. 8.0–1) and metafor package (v. 4.6-0) in R (v. 4.4.2). A p value of less than 0.05 was considered to indicate statistical significance. Owing to differences among the studies (including the use of different tracers and data processing methods), a random effects model was employed to obtain the SMD and 95% confidence intervals (95% CI). Heterogeneity was assessed using I^2 (0–49% was considered low heterogeneity, whereas heterogeneity greater than 50% was considered high heterogeneity [19]).

With respect to the tau PET tracer uptake across brain regions in different tauopathies, for each brain region in each comparison group, a meta-analysis could be conducted if at least five studies met the inclusion criteria, as recommended for random effects meta-analysis [20]. A forest plot was constructed to visualize the results of the SMD and 95% CI for each brain region. For the diagnostic performance of tau PET in tauopathies, a meta-analysis could be conducted if at least five contingency tables met the inclusion criteria. Pooled SE, SP, and AUC values were calculated to assess diagnostic performance overall, and stratified operating characteristic (SROC) curves and forest plots were generated to visualize the results.

Additionally, to reduce heterogeneity and investigate its sources, subgroup analyses were conducted based on the following factors: (1) type of study outcome; (2) atlas used for brain region division (if applicable); and (3) type of tracer (specific types and first/second generation).

Results

Study selection and characteristics

The systematic search identified 4,031 records across three databases (MEDLINE, Embase, and Web of Science). After 1,766 duplicates were removed through Zotero software (v. 7.0.13), 2,265 titles/abstracts were screened for automated

deduplication with manual verification. Following the exclusion of 2,010 irrelevant studies, 255 full-text articles underwent eligibility assessment. Ultimately, 80 studies met the inclusion criteria (Fig. 1).

The study characteristics are summarized in Tables 1 and 2 and Supplementary Table 1. The 80 studies (56.3% prospective; 23.8% multicenter) originated from 11 countries and included 9,166 participants (4,583 patients: AD = 1,944; PSP = 444; CBS = 123; AD/MCI = 449; and 4,583 healthy controls [HCs]). The mean patient age was 69.78 ± 9.26 years, with 34.2% female representation (gender was not reported in 6 studies). Seven studies utilized open-access neuroimaging repositories (e.g., ADNI). Most studies selected patients on the basis of standard clinical diagnosis. Twelve tau tracers were analyzed, predominantly first-generation tracers, namely, [^{18}F]AV-1451 (35.0%), [^{18}F]THK-5351 (18.8%), and [^{18}F]FDDNP (10.0%), complemented by second-generation tracers, such as [^{18}F]PI-2620 (12.5%), [^{18}F]MK-6240 (7.5%), and [^{18}F]PM-PBB3 (11.3%). The quantification methods included a standardized uptake value ratio (SUVR) (81.3%), distribution volume ratio (DVR) (13.8%), and binding potential (BPND) (5.0%), with the cerebellar gray matter as the reference region in 73.8% of the studies.

Table 2
Reference Standard and data Characteristics of included studies (n = 80).

Table 1. Tracer type, study design and patient characteristics of included studies (n = 80)

Author. [ref] year	Tracer	Study design	Subjects					Age (average (SD) or range, years)	Female (%)
			AD	PSP	CBS	AD/MCI	HC		
Baker et al. [54] 2017	[18F]AV-1451	P	15	NR	NR	NR	28	AD: 64 ± 8.0 HC: 68 ± 22.3	AD: 66.67 HC:60.71
Barret et al. [55] 2017	[18F]AV-1451	P	8	NR	NR	NR	8	AD: 64.9 ± 8.6 HC: 47.2 ± 17.8	AD: 62.50 HC: 50.00
Barrio et al. [56] 2015	[18F]FDDNP	R	24	NR	NR	NR	28	AD: 73.5 ± 9.7 HC: 64.3 ± 14.1	AD: 50.00 HC: 32.14
Barthélemyet al. [57] 2022	[18F]GTP1	P	12	NR	NR	NR	11	AD: 70.6 ± 6.1 HC: 63.4 ± 8.0	AD: 66.67 HC: 45.45
Blazhenets et al. [58] 2023	[18F]PI-2620	R	NR	14	11	16	23	PSP:70 ± 7 CBS:66 ± 7 AD/MCI: 73 ± 9 HC: 69 ± 11	PSP: 21.43 CBS: 72.73 AD/MCI: 37.50 HC: 61.0
Brendel et al. [59] 2018	[18F]THK-5351	R	NR	11	NR	NR	9	PSP: 68.4 ± 7.4 HC: 71.6 ± 6.6	PSP: 54.55 HC: 44.44
Bun et al. [60] 2022	[18F]PI-2620	P	7	NR	NR	NR	7	AD: 70.7 ± 9.1 HC: 71.1 ± 6.6	AD: 42.86 HC: 42.86
Chen et al. [61] 2018	[18F]FDDNP	R	24	NR	NR	NR	28	AD: 77 (50–86) HC: 62.5 (30–84)	AD: 50.00 HC: 27.78
Cho et al. [62] 2016	[18F]AV-1451	P	20	NR	NR	NR	20	AD: 74.3 ± 9.5 HC: 71.5 ± 7.5	AD: 80.00 HC: 55.00

Table 1. Tracer type, study design and patient characteristics of included studies (n = 80)

Author. [ref] year	Tracer	Study design	Subjects					Age (average (SD) or range, years)	Female (%)
			AD	PSP	CBS	AD/MCI	HC		
Cho et al. [63] 2017	[18F]AV-1451	P	NR	14	NR	NR	15	PSP: 70.8 ± 6.2 HC: 68.7 ± 5.3	PSP: 7.14 HC: 46.67
Cho et al. [64] 2017	[18F]AV-1451	P	32	NR	NR	NR	30	AD: 73.9 ± 8.1 HC: 70.4 ± 7.6	AD: 84.38 HC: 66.67
Coakeley et al. [65] 2017	[18F]AV-1451	P	NR	6	NR	NR	10	PSP: 72.2 ± 6.8 HC: 65.9 ± 9.9	PSP: 66.67 HC: 80.00
Ezura et al. [66] 2021	[18F]THK-5351	P	10	9	7	NR	9	AD: 75.6 ± 10.0 PSP: 74.1 ± 5.28 CBS: 69.1 ± 4.85 HC: 71.0 ± 6.44	AD: 30.00 PSP: 0 CBS: 71.43 HC: 44.44
Gonzalez et al. [67] 2021	[18F]AV-1451	R	61	NR	NR	NR	410	AD: 77.3 ± 8.4 HC: 73.6 ± 7.3	AD: 60.66 HC: 41.2
Harada et al. [68] 2015	[18F]THK-5117	P	5	NR	NR	NR	5	NR	NR
Harrison et al. [69] 2019	[18F]AV-1451	R	19	NR	NR	NR	42	AD: 63.1 ± 10.3 HC: 77.6 ± 4.6	AD: 63.16 HC: 59.52
Hsu et al. [70] 2020	[18F]THK-5351	P	NR	17	NR	NR	28	PSP: 68.9 ± 6.5 HC: 66.2 ± 4.5	PSP: 47.06 HC: 47.06
Hsu et al. [71] 2020	[18F]PM-PBB3 [18F]AV-1451	P	12	NR	NR	NR	10	AD: 72.5 ± 10.0 HC: 56.0 ± 11.8	AD: 60.00 HC: 41.67
Ishiki et al. [72] 2017	[18F]THK-5351	P	13	3	NR	NR	9	AD: 76.6 ± 9.1	AD: 30.77 PSP: 0

Table 1. Tracer type, study design and patient characteristics of included studies (n = 80)

Author. [ref] year	Tracer	Study design	Subjects					Age (average (SD) or range, years)	Female (%)
			AD	PSP	CBS	AD/MCI	HC		
								PSP: 78.3 ± 3.7 HC: 71.6 ± 6.6	HC: 44.44
Jantarato et al. [73] 2021	[18F]PI-2620	P	7	NR	NR	NR	26	AD: 64.6 ± 6.1 HC: 63.8 ± 4.6	AD: 57.14 HC: 70.00
Jeon et al. [74] 2019	[18F]THK-5351	P	83	NR	NR	NR	60	AD: 67.6 ± 10.1 HC: 66.2 ± 11.1	AD: 71.08 HC: 48.33
Johnson et al. [75] 2016	[18F]AV-1451	R	6	NR	NR	NR	56	AD: 63 ± 12 HC: 75 ± 6	AD: 33.33 HC: 85.71
Kang et al. [76] 2017	[18F]THK-5351	P	51	NR	NR	NR	43	AD: 70.8 ± 10.8 HC: 66.4 ± 7.9	AD: 52.94 HC: 76.5
Kepe et al. [77] 2013	[18F]FDDNP	P	NR	15	NR	NR	5	PSP: 68.3 ± 7.5 HC: 68.0 ± 8.6	PSP: 46.67 HC: 40.00
Kikuchi et al. [78] 2016	[18F]THK-5351	P	NR	NR	5	NR	8	CBS: 69.2 ± 7.0 HC: NR	CBS: 80.00 HC: NR
Krishnadas et al. [79] 2023	[18F]MK-6240	R	25	NR	NR	NR	133	AD: 69.4 ± 8.1 HC: 75.7 ± 5.6	AD: 48.00 HC: 49.62
Lagarde et al. [80] 2019	[18F]AV-1451	R	16	NR	NR	NR	11	AD: 67.7 ± 7.1 HC: 68.9 ± 3.3	AD: 50.00 HC: 63.63
Lagarde et al. [81] 2022	[18F]AV-1451	R	36	NR	NR	NR	15	AD: 68.1 ± 6.7 HC: 68.7 ± 3.6	AD: 47.22 HC: 66.67
Lee et al. [82] 2018	[18F]AV-1451	P	25	NR	NR	NR	25	AD: 74.0 ± 4.0	AD: 92.00 HC: 60.00

Table 1. Tracer type, study design and patient characteristics of included studies (n = 80)

Author. [ref] year	Tracer	Study design	Subjects					Age (average (SD) or range, years)	Female (%)
			AD	PSP	CBS	AD/MCI	HC		
								HC: 73.2 ± 3.5	
Li et al. [83] 2021	[18F]AV-1451	P	4	7	9	NR	10	AD: 70.0 ± 8.8 PSP: 70.0 ± 6.5 CBS: 63.3 ± 13.2 HC: 60.1 ± 10.4	AD: 25.00 PSP: 57.14 CBS: 77.78 HC: 80.00
Liu et al. [84] 2023	[18F]PM-PBB3	P	NR	148	NR	NR	20	PSP: 65.7 ± 6.8 HC: 56.7 ± 7.3	PSP: 43.92 HC: 70.00
Lu et al. [85] 2020	[18F]PM-PBB3	P	19	NR	NR	NR	11	AD: 61.8 ± 11.3 HC: 61.8 ± 4.6	AD: 63.16 HC: 36.36
Meindl et al. [86] 2024	[18F]PI-2620	R	10	15	NR	NR	15	AD: 67 PSP: 69 HC: 70	AD: 80.00 PSP: 53.33 HC: 50.00
Mueller et al. [87] 2020	[18F]PI-2620	P	12	NR	NR	NR	10	AD: 68.5 ± 9.8 HC: 59.2 ± 7.8	AD: 33.33 HC: 30.00
Nam et al. [88] 2018	[18F]THK-5351	R	21	NR	NR	NR	24	AD: 76.3 ± 6.1 HC: 73.96 ± 4.7	AD: 66.67 HC: 54.17
Ng et al. [89] 2019	[18F]THK-5351	P	NR	4	NR	NR	2	PSP: 78.8 ± 8.8 HC: 64.5 ± 0.5	PSP: 25.00 HC: 50.00
Niccolini et al. [90] 2018	[18F]AV-1451	R	NR	NR	11	NR	20	CBS: 69.2 ± 6.8 HC: 72.4 ± 4.8	CBS: 54.55 HC: 50.00
Nihashi et al. [91] 2022	[18F]THK-5351	R	17	NR	NR	NR	11	AD: 68(64–75)	AD: 47.06 HC: 53.13

Table 1. Tracer type, study design and patient characteristics of included studies (n = 80)

Author. [ref] year	Tracer	Study design	Subjects					Age (average (SD) or range, years)	Female (%)
			AD	PSP	CBS	AD/MCI	HC		
								HC: 74.5(69–76)	
Okamura et al. [92] 2014	[18F]THK-5105	P	8	NR	NR	NR	8	AD: 74.1 ± 6.9 HC: 70.5 ± 4.4	AD: 62.50 HC: 62.50
Hauer et al. [93] 2023	[18F]RO-948	R	NR	23	NR	NR	61	PSP: 69.1 ± 8.4 HC: 71.9 ± 8.8	PSP: 56.52 HC: 54.10
Pascoal et al. [94] 2020	[18F]MK-6240	R	54	NR	NR	NR	168	AD: 66.3 ± 9.7 HC: 62.3 ± 19.9	AD: 55.56 HC: 65.48
Santillo et al. [95] 2023	[18F]RO-948	P	13	NR	NR	NR	13	AD: 67.5 ± 5.2 HC: 66.9 ± 5.1	AD: 53.85 HC: 61.54
Small et al. [96] 2006	[18F]FDDNP	P	25	NR	NR	NR	30	AD: 73 ± 9 HC: 64 ± 15	AD: 52.00 HC: 40.00
Smith et al. [35] 2017	[18F]AV-1451	R	NR	NR	8	NR	17	CBS: 67.5 ± 8.0 HC: 73 ± 6	NR
Smith et al. [97] 2017	[18F]AV-1451	P	NR	11	NR	NR	11	PSP: 70.7 ± 2.2 HC: 70.9 ± 1.9	NR
Tagai et al. [98] 2022	[18F]PM-PBB3	R	23	40	NR	NR	40	AD: 66.2 ± 10.0 PSP: 70.4 ± 6.4 HC: 68.6 ± 5.7	AD: 52.17 PSP: 45.00 HC: 37.50
Tauber et al. [99] 2013	[18F]FDDNP	P	7	NR	NR	NR	8	AD: 79.3 ± 3.6 HC: 75.7 ± 3.9	AD: 57.14 HC: 62.50
Tolboom et al. [100] 2009	[18F]FDDNP	P	14	NR	NR	NR	13	AD: 63 ± 7	AD: 42.86

Table 1. Tracer type, study design and patient characteristics of included studies (n = 80)

Author. [ref] year	Tracer	Study design	Subjects					Age (average (SD) or range, years)	Female (%)
			AD	PSP	CBS	AD/MCI	HC		
								HC: 67 ± 7	HC: 38.46
Tsai et al. [101] 2019	[18F]AV-1451	R	NR	NR	7	NR	53	NR	NR
Villemagne et al. [102] 2014	[18F]THK-523	P	10	NR	NR	NR	10	AD: 75.6 ± 9.5 HC: 77.4 ± 10.0	AD: 60.00 HC: 70.00
Wardak et al. [103] 2010	[18F]FDDNP	R	12	NR	NR	NR	9	AD: 74 ± 8 HC: 69 ± 8	AD: 50.00 HC: 33.33
Wolters et al. [104] 2020	[18F]AV-1451	R	65	NR	NR	NR	50	AD: 66 ± 8 HC: 66 ± 8	AD: 46.15 HC: 48.00
Wong et al. [105] 2018	[18F]RO-948	P	11	NR	NR	NR	10	NR	NR
Yoon et al. [106] 2018	[18F]THK-5351	R	13	NR	NR	NR	15	AD: 73.2 ± 12.1 HC: 67.1 ± 5.1	AD: 61.54 HC: 73.33
Dang et al. [107] 2023	[18F]AV-1451	R	83	NR	NR	NR	38	AD: 64.9 ± 9.2 HC: 64.3 ± 9.9	AD: 50.60 HC: 31.58
Jiao et al. [108] 2023	[18F]AV-1451	R	121	NR	NR	NR	211	AD: 72.1 ± 7.5 HC: 71.2 ± 6.4	AD: 54.55 HC: 62.56
	[18F]PM-PBB3		36	NR	NR	NR	36	AD: 58.2 ± 9.6 HC: 58.5 ± 8.2	AD: 61.36 HC: 55.56
Lin et al. [109] 2023	[18F]PM-PBB3	P	NR	NR	NR	34	12	AD/MCI: 71.7 ± 4.7 HC: 64.6 ± 6.7	AD/MCI: 61.76 HC: 50
Maass et al. [110] 2017	[18F]AV-1451	R	NR	NR	NR	60	86	AD/MCI: 64.2 ± 8.4 HC: 71.6 ± 15.8	AD/MCI: 61.67 HC:53.49
	[18F]AV-1451		NR	NR	NR	28	42	AD/MCI: 79.0 ± 6.4	AD/MCI: 71.43

Table 1. Tracer type, study design and patient characteristics of included studies (n = 80)

Author. [ref] year	Tracer	Study design	Subjects					Age (average (SD) or range, years)	Female (%)
			AD	PSP	CBS	AD/MCI	HC		
								HC: 74 ± 6	HC: 50.00
Mattsson et al. [111] 2018	[18F]AV-1451	P	39	NR	NR	NR	30	AD: 71.3 ± 7.2 HC: 74.7 ± 5.5	AD: 46.15 HC: 50.00
Rullmann et al. [112] 2022	[18F]PI-2620	P	38	NR	NR	NR	26	AD: 69 ± 9 HC: 67 ± 11	AD: 55.26 HC: 50
Seibyl et al. [113] 2023	[18F]MK-6240	R	NR	NR	NR	46	52	AD/MCI: 72.0 ± 9.0 HC: 66.4 ± 12.1	AD/MCI: 32.61 HC: 51.92
Tolboom et al. [114] 2010	[18F]FDDNP	P	16	NR	NR	NR	15	AD: 63 ± 6 HC: 67 ± 6	NR
Yokoi et al. [115] 2018	[18F]THK-5351	R	23	NR	NR	NR	24	AD: 68.6 ± 7.8 HC: 65.4 ± 7.3	AD: 82.61 HC: 66.67
Brendel et al. [15] 2020	[18F]PI-2620	P	8	60	NR	NR	10	AD: 69 ± 10 PSP: 71 ± 7 HC: 67 ± 7	AD: 50.00 PSP: 45.00 HC: 80.00
Chanisa et al. [116] 2021	[18F]THK-5351	P	15	NR	NR	NR	24	AD: 60.7 ± 6.8 HC: 59.7 ± 10.8	AD: 73.33 HC: 54.17
Chen et al. [117] 2018	[18F]THK-5351	R	9	NR	NR	NR	9	AD:76 (58, 88) HC: 73(61,90)	AD: 33.33 HC: 22.22
	[18F]AV-1451		12	NR	NR	NR	20	AD: 78 (60, 90) HC: 73 (68, 82)	AD: 50.00 HC: 45.00
Endo et al. [118] 2019	[11C]PBB3	R	NR	13	NR	NR	13	PSP: 71.3 ± 7.7 HC: 68.0 ± 4.3	PSP: 30.77 HC: 30.77

Table 1. Tracer type, study design and patient characteristics of included studies (n = 80)

Author. [ref] year	Tracer	Study design	Subjects					Age (average (SD) or range, years)	Female (%)
			AD	PSP	CBS	AD/MCI	HC		
Gerard et al. [119] 2024	[18F]MK-6240	P	19	NR	NR	NR	17	AD: 70.0 ± 8.4 HC: 65.7 ± 8.9	AD: 47.37 HC: 52.94
Kim et al. [120] 2021	[18F]THK-5351	P	26	NR	NR	NR	32	AD: 63.6 ± 10.6 HC: 69.4 ± 6.0	AD: 57.69 HC: 65.63
Leuzy et al. [121] 2020	[18F]RO-948	P	100	NR	NR	NR	257	AD: 73.5 ± 6.7 HC: 65.8 ± 12.1	AD: 43.00 HC: 54.47
Leuzy et al. [122] 2021	[18F]AV-1451	R	159	NR	NR	NR	638	AD:70.7 ± 10.4 HC: 69.7 ± 9.0	AD: 59.75 HC: 57.05
	[18F]RO-948		142	NR	NR	NR	208	AD: 74.1 ± 6.7 HC: 75.3 ± 5.9	AD: 54.23 HC: 55.77
	[18F]MK-6240		50	NR	NR	NR	218	AD: 66.1 ± 10.0 HC: 61.6 ± 19.8	AD: 56.00 HC: 66.06
Li et al. [123] 2021	[18F]PM-PBB3	P	NR	20	NR	NR	13	PSP: 63.0 ± 7.4 HC: 60.6 ± 4.2	PSP: 35.00 HC: 38.46
Liu et al. [124] 2023	[18F]PM-PBB3	P	20	16	20	NR	20	AD: 65.6 ± 8.8 PSP: 64.0 ± 7.3 CBS: 68.8 ± 8.9 HC: 56.7 ± 7.3	AD: 65.00 PSP: 43.75 CBS: 65.00 HC: 70.00
Messerschmidt et al. [125] 2022	[18F]PI-2620	R	NR	36	NR	NR	10	PSP: 71 ± 8 HC: 67 ± 7	PSP: 44.44 HC: 80.00

Table 1. Tracer type, study design and patient characteristics of included studies (n = 80)

Author. [ref] year	Tracer	Study design	Subjects					Age (average (SD) or range, years)	Female (%)
			AD	PSP	CBS	AD/MCI	HC		
Ossenkoppele et al. [126] 2018	[18F]AV-1451	R	179	NR	NR	NR	160	AD: 68.8 ± 9.6 HC: 69.1 ± 9.5	AD: 40.78 HC: 40.63
Palleis et al. [127] 2021	[18F]PI-2620	P	NR	NR	45	NR	14	CBS: 71.5 ± 7.6 HC: 67.4 ± 9.5	CBS: 60.00 HC: 60.00
Schonhaut et al. [128] 2017	[18F]AV-1451	R	NR	33	NR	NR	46	PSP: 69.6 ± 5.7 HC: 69.6 ± 5.4	PSP: 30.30 HC: 45.65
Song et al. [129] 2021	[18F]PI-2620	R	NR	37	NR	NR	10	PSP: 70.8 ± 6.3 HC: 67.0 ± 7.4	PSP: 40.54 HC: 80.00
Tagai et al. [130] 2021	[18F]PM-PBB3	P	NR	18	NR	17	23	PSP: 70.7 ± 11.9 AD/MCI: 71.2 ± 6.6 HC: 65.2 ± 5.0	PSP: 58.82 AD/MCI: 33.33 HC: 47.83
Zou et al. [131] 2021	[18F]MK-6240	R	NR	NR	NR	121	199	AD/MCI: 70.2 ± 8.8 HC: 66.0 ± 5.5	AD/MCI: 47.93 HC: 70.35
	[18F]AV-1451		NR	NR	NR	127	319	AD/MCI: 75.3 ± 8.3 HC: 73.5 ± 8.2	AD/MCI: 43.31 HC: 57.37

AD Alzheimer's disease, **PSP** progressive supranuclear palsy, **CBS** corticobasal syndrome, **AD/MCI** AD and mild cognitive impairment mixed, **HC** healthy control, **[18F]AV-1451** 7-(6-Fluoro-3-pyridinyl)-5H-pyrido[4,3-b]indole, **[18F]FDDNP** 2-(1-(6-((2-((18)F)fluoroethyl)(methyl)amino)-2- naphthyl)ethylidene)malononitrile, **[18F]GTP1** 2-[4-(2,2-dideuterio-2-(18F)fluoranylethyl)piperidin-1-yl]pyrimido[1,2-a]benzimidazole, **[18F]PI-2620** 11-(2-(18F)fluoranylpyridin-4-yl)-4,8,10-triazatricyclo[7.4.0.02,7]trideca-1(9),2(7),3,5,10,12-hexaene, **[18F]THK-5351** (2S)-1-(18F)fluoranyl-3- [2-[6-(methylamino)pyridin-3-yl]quinolin-6-yl]oxypropan-2-ol, **[18F]PM-PBB3** 1-(18F)fluoranyl-3-[[2-[(1E,3E)-4- [6-(methylamino)pyridin-3-yl]buta- 1,3-dienyl]-1,3-benzothiazol-6-yl]oxy]propan-2-ol, **[18F]MK-6240** 6-(18F)fluoranyl-3-pyrrolo[2,3-c]pyridin-1-ylisoquinolin-5-amine, **[18F]RO-948** RO6958948, **[18F]THK-5117** 1-(18F)fluoranyl-3-[2-[4-(methylamino)phenyl]quinolin-6-yl]oxypropan-2-ol, **[18F]THK-5105** (2S)-1-[2-[4-(dimethylamino)phenyl]quinolin-6-yl]oxy-3-(18F)fluoranylpropan-2-ol, **[18F]THK-523** 4-[6-(2-(18F)fluoranylethoxy)quinolin-2-yl]aniline, **[11C]PBB3** 2-[(1E,3E)-4- [6-((111C)methylamino)pyridin-3-yl]buta-1,3-dienyl]-1,3-benzothiazol-6-ol, **P** prospective study, **R** retrospective study, **NR** not reported.

Author. [ref] year	Reference Standard	Outcome	Atlas	Reference brain region	Source of data	Data range
Baker et al. [54] 2017	NR	DVR	DK	Cerebellar gray matter	Lawrence Berkeley National Laboratory	NR
Barret et al. [55] 2017	NINCDS-ADRDA 2011	SUVR	Hammers	Cerebellar gray matter	Molecular NeuroImaging LLC	NR
Barrio et al. [56] 2015	NINCDS-ADRDA 1984 APA 2000	DVR	DK	Cerebellar gray matter	University of California, Los Angeles	NR
Barthélemyet al. [57] 2022	NINCDS-ADRDA 2011	SUVR	AAL	Cerebellar gray matter	ClinicalTrials.gov ID NCT02640092	2015.12.23-2019.06.11
Blazhenets et al. [58] 2023	NINCDS-ADRDA 2011 MDS 2017 the Armstrong criteria	SUVR	DK the atlas of Ilinsky et al.[1]	Inferior cerebellar gray matter	(a) the multicenter 4 Repeat Tauopathy Neuroimaging Initiative-Cycle 2 cohort (b) University of California, San Francisco, Alzheimer's Disease Research Center	As of 2022.12.15
Brendel et al. [59] 2018	NINDS-SPSP 1996	SUVR	Hammers	cerebellar gray matter	(a) the Departments of Neurology, Ludwig-Maximilians-Universität München and Technical University of Munich (b) Tohoku University School of Medicine	NR
Bun et al. [60] 2022	NINCDS-ADRDA 2011	SUVR	DK	cerebellar gray matter	(a) Keio University Hospital (b) The patient recruitment agency (3H Medi Solution Inc., Tokyo, Japan)	NR
Chen et al. [61] 2018	NINCDS-ADRDA 1984 APA 2000	DVR	DK	cerebellum	University of California, Los Angeles	NR
Cho et al. [62] 2016	NINCDS-ADRDA 1984	SUVR	DK	cerebellum	the Memory Disorder Clinic of Gangnam Severance Hospital	2015.01-2015.08
Cho et al. [63] 2017	NINDS-SPSP 1996	SUVR	DK	cerebellar gray matter	the Memory Disorder Clinic of Gangnam Severance Hospital	2015.05-2016.06

Author. [ref] year	Reference Standard	Outcome	Atlas	Reference brain region	Source of data	Data range
Cho et al. [64] 2017	NINCDS-ADRDA 1984	SUVR	DK	cerebellar gray matter	the Memory Disorder Clinic of Gangnam Severance Hospital	2015.01-2016.02
Coakeley et al. [65] 2017	NINDS-SPSP 1996	SUVR	Talairach Atlas	cerebellar gray matter	University of Toronto	NR
Ezura et al. [66] 2021	NINCDS-ADRDA 1984 NINDS-SPSP 1996 the modified Cambridge criteria[2]	SUVR	AAL	cerebellar gray matter	Tohoku University Hospital	NR
Gonzalez et al. [67] 2021	NINCDS-ADRDA 2011	SUVR	DK	cerebellar gray matter	ADNI-3	NR
Harada et al. [68] 2015	NINCDS-ADRDA 2011	SUVR	AAL	cerebellar gray matter	Tohoku University Hospital	NR
Harrison et al. [69] 2019	NINCDS-ADRDA 2011	SUVR	DK	white matter	(a) Berkeley Aging Cohort Study (b) University of California, San Francisco Alzheimer's Disease Research Center	NR
Hsu et al. [70] 2020	MDS 2017	SUVR	the Harvard-Oxford cortical structural atlas[3]	cerebellar gray matter	NR	NR
Hsu et al. [71] 2020	NINCDS-ADRDA 1984	SUVR	the Harvard-Oxford cortical structural atlas[3]	[18F]AV-1451: cerebellum [18F]PM-PBB3: cerebellar gray matter	Chang Gung Memorial Hospital	NR
Ishiki et al. [72] 2017	NINCDS-ADRDA 2011 NINDS-SPSP 1996	SUVR	AAL	cerebellar gray matter	Tohoku University School of Medicine	NR
Jantarato et al. [73] 2021	NINCDS-ADRDA 2011	SUVR	AAL	cerebellum	National Cyclotron and PET Centre, Chulabhorn Hospital	NR

Author. [ref] year	Reference Standard	Outcome	Atlas	Reference brain region	Source of data	Data range
Jeon et al. [74] 2019	NINCDS-ADRDA 1984	SUVR	DK	cerebellar gray matter	(a) memory disorder clinic at Samsung Medical Center; (b) Gachon University Gil Medical Center	2015.03-2017.11
Johnson et al. [75] 2016	Harvard Aging Brain Study	SUVR	DK	cerebellum	(a)the Harvard Aging Brain Study (b)Memory Disorders Clinics at the Massachusetts General and Brigham and Women's Hospitals; (c)the Massachusetts Alzheimer's Disease Research Center.	No
Kang et al. [76] 2017	NINCDS-ADRDA 1984	SUVR	DK	cerebellar gray matter	Gachon University Gil Medical Center	2015.03-2016.12
Kepe et al. [77] 2013	NINDS-SPSP 1996	DVR	NR	cerebellar gray matter	University of California at Los Angeles	NR
Kikuchi et al. [78] 2016	the modified Cambridge criteria	SUVR	Hammers	cerebellar gray matter	Tohoku University School of Medicine	NR
Krishnadas et al. [79] 2023	NINCDS-ADRDA 2011	SUVR	DK	cerebellar gray matter	(a)the Australian Imaging Biomarkers and Lifestyle flagship study of ageing (AIBL) (b)The Australian Dementia Network (ADNeT)	As of 2022.09
Lagarde et al. [80] 2019	positive CSF biomarkers PiB-PET (Global cortical index > 1.45) CDR scale ≤ 1	SUVR	AAL	cerebellar gray matter	Shatau7-Imatau study	NR
Lagarde et al. [81] 2022	positive CSF biomarkers PiB-PET (Global cortical index > 1.45) CDR scale ≤ 1	SUVR	AAL	cerebellar gray matter	Shatau7-Imatau study	2016.03-2019.11

Author. [ref] year	Reference Standard	Outcome	Atlas	Reference brain region	Source of data	Data range
Lee et al. [82] 2018	NINCDS-ADRDA 1984	SUVR	DK	cerebellar gray matter	the Memory Disorder Clinic of Gangnam Severance Hospital	NR
Li et al. [83] 2021	NINCDS-ADRDA 2011 MDS 2017 the Armstrong criteria	SUVR	DK	cerebellar gray matter	the movement disorder or dementia special clinics of National Taiwan University Hospital	NR
Liu et al. [84] 2023	MDS 2017	SUVR	(a) Multicontrast PD25 template (b) AAL3 (c) Wake Forest University PickAtlas	cerebellar gray matter	the Movement Disorders Clinic, Department of Neurology, Huashan Hospital, Fudan University	2019.05-2022.01
Lu et al. [85] 2020	NINCDS-ADRDA 2011	SUVR	Hammers	cerebellar gray matter	Huashan Hospital, Fudan University	2018.11-2019.11
Meindl et al. [86] 2024	Jack CR Jr et al.[4] MDS 2017	DVR	AAL	cerebellum	Department of Nuclear Medicine, Ludwig Maximilian University Hospital	NR
Mueller et al. [87] 2020	NINCDS-ADRDA 1984 APA 1994	SUVR	AAL	Cerebellar gray matter, excluding vermis and anterior lobe surrounding vermis	NR	NR
Nam et al. [88] 2018	NINCDS-ADRDA 1984	SUVR	DK	cerebellar gray matter	Gachon University	NR
Ng et al. [89] 2019	NINDS-SPSP 1996	SUVR	the alas of Xiao et al.[5]	cerebellar gray matter	McGill University Research Center for Studies in Aging	NR
Niccolini et al. [90] 2018	the Armstrong criteria	SUVR	DK	cerebellar gray matter excluding the dentate nucleus	(a) specialist movement disorders clinics at King's College Hospital NHS Foundation Trust (b) National Hospital of Neurology and Neurosurgery (c) ADNI	NR

Author. [ref] year	Reference Standard	Outcome	Atlas	Reference brain region	Source of data	Data range
Nihashi et al. [91] 2022	NINCDS-ADRDA 2011	SUVR	AAL	cerebellar gray matter	(a) National Center for Geriatrics and Gerontology (a) Multimodal NeuroImaging for Alzheimer's disease Diagnosis Study (b) A dementia study by amyloid and tau PET	NR
Okamura et al. [92] 2014	NINCDS-ADRDA 1984	SUVR	AAL	cerebellar gray matter	NR	NR
Hauer et al. [93] 2023	MDS 2017	SUVR	DK	the inferior cerebellar gray matter	Neurology and Memory clinics at Skåne University Hospital	NR
Pascoal et al. [94] 2020	NR	SUVR	DK	the inferior cerebellum	Translational Biomarkers of Aging and Dementia cohort, McGill University	NR
Santillo et al. [95] 2023	NR	SUVR	DK	the inferior cerebellar gray matter	BioFINDER-2 study	2017–2020
Small et al. [96] 2006	NINCDS-ADRDA 1984 APA 2000	DVR	Talairach Atlas	cerebellum	David Geffen School of Medicine at the University of California	NR
Smith et al. [35] 2017	the modified Cambridge criteria the Armstrong criteria	SUVR	DK	cerebellar gray matter	BioFINDER-2 study	NR
Smith et al. [97] 2017	NINDS-SPSP 1996	SUVR	AAL	Cerebellar gray matter, excluding the dentate nucleus	Neurology Clinic and the Memory Clinic at Skåne University Hospital, Malmo, and Lund, Sweden	NR
Tagai et al. [98] 2022	NINCDS-ADRDA 1984 MDS 2017	SUVR	DK	cerebellum	UMIN Clinical Trials Registry (UMIN–CTR; IDs 000030248, 000034546, 000033808, 000030319)	NR
Tauber et al. [99]	NINCDS-ADRDA	SUVR	Talairach Atlas	cerebellum	NR	NR

Author. [ref] year	Reference Standard	Outcome	Atlas	Reference brain region	Source of data	Data range
2013	1984					
Tolboom et al. [100] 2009	NINCDS-ADRDA 1984	BPND	Talairach Atlas	cerebellar gray matter	VU University Medical Centre	NR
Tsai et al. [101] 2019	the Armstrong criteria	SUVR	DK	cerebellar gray matter	University of California San Francisco	2014.09-2017.08
Villemagne et al. [102] 2014	NINCDS-ADRDA 1984	SUVR	AAL	cerebellar gray matter	NR	NR
Wardak et al. [103] 2010	NINCDS-ADRDA 1984	DVR	NR	cerebellar gray matter	David Geffen School of Medicine at the University of California	NR
Wolters et al. [104] 2020	NINCDS-ADRDA 2011	BPND	Hammers	cerebellar gray matter	Amsterdam Dementia Cohort	NR
Wong et al. [105] 2018	NINCDS-ADRDA 1984	SUVR	DK	cerebellar cortex, excluding the vermis and upper 6 mm to reduce contamination from the supratentorial regions	Johns Hopkins Medical Institutions	NR
Yoon et al. [106] 2018	NINCDS-ADRDA 1984	SUVR	AAL	cerebellar gray matter	Gachon University Gil Medical Center	2015.04-2016.04
Dang et al. [107] 2023	NINCDS-ADRDA 1984	SUVR	NR	cerebellar gray matter	Beijing Aging Brain Rejuvenation Initiative project	NR
Jiao et al. [108] 2023	NINCDS-ADRDA 2011	SUVR	AAL	cerebellum	(a) Huashan hospital, Fudan university (b) ADNI	NR
Lin et al.[109] 2023	NIA-AD 2011 Jack CR Jr et al.[4]	SUVR	NR	the inferior cerebellar gray matter	Chang Gung Memorial Hospital	NR
Maass et al. [110] 2017	NINCDS-ADRDA 2011 NIA-AD 2011	SUVR	DK	the inferior cerebellar gray matter	(a) University of California San Francisco Memory and Aging Center (b) ADNI	NR

Author. [ref] year	Reference Standard	Outcome	Atlas	Reference brain region	Source of data	Data range
Mattsson et al. [111] 2018	NINCDS-ADRDA 1984	SUVR	DK	cerebellar gray matter	BioFINDER-2 study	NR
Rullmann et al. [112] 2022	NINCDS-ADRDA 1984	DVR	AAL	the inferior cerebellum	(a)University Hospital of Munich (b)University of Leipzig (c)Melbourne, Australia (d)New Haven, USA	NR
Seibyl et al. [113] 2023	NR	SUVR	NR	NR	Cerveau Technologies	NR
Tolboom et al. [114] 2010	NR	BPND	NR	NR	NR	NR
Yokoi et al. [115] 2018	NINCDS-ADRDA 2011	SUVR	Hammers	cerebellum	(a)Nagoya University Hospital (b)Dementia Center of Meitetsu Hospital	NR
Brendel et al. [15] 2020	MDS 2017	SUVR	the atlas of the basal ganglia[6] The Brainnetom Atlas[7] Hammers	cerebellum excluding the dentate nucleus and the central cerebellar white matter as well as the superior and the posterior cerebellar layers	German Clinical Trials Register (DRKS00016920)	2016.12-2019.10
Chanisa et al. [116] 2021	NINCDS-ADRDA 2011	SUVR	AAL	cerebellum	National Cyclotron and PET Centre, Chulabhorn Hospital	NR
Chen et al. [117] 2018	NINCDS-ADRDA 2011	SUVR	DK	cerebellar gray matter	(a) memory clinic of Tohoku University Hospital (b) ADNI	NR
Endo et al. [118] 2019	MDS 2017	BPND	AAL	cerebellar gray matter	(a) Chiba University Hospital and affiliated hospitals (b) National Institute of Radiological Sciences	2012.07-2015.10
Gerard et al. [119]	amyloid status	SUVR	Hammers	cerebellar gray matter	the Memory Clinic of the Cliniques	2019.06-

Author. [ref] year	Reference Standard	Outcome	Atlas	Reference brain region	Source of data	Data range
2024	positive MMSE score < 24				Universitaires Saint Luc in Brussels, Belgium	2023.02
Kim et al. [120] 2021	NINCDS-ADRDA 2011	SUVR	DK	cerebellar gray matter	(a)Asan Medical Center (b)Samsung Medical Center	NR
Leuzy et al. [121] 2020	Jack CR Jr et al.[4]	SUVR	DK	the inferior cerebellar gray matter	BioFINDER-2 study	NR
Leuzy et al. [122] 2021	Jack CR Jr et al.[4]	SUVR	DK	the inferior cerebellar gray matter	the Memory Disorder Clinic of Gangnam Severance Hospital BioFINDER study University of California San Francisco Alzheimer Disease Research Center BioFINDER-2 study McGill University Avid Radiopharmaceuticals Study	NR
Li et al. [123] 2021	MDS 2017	SUVR	Wake Forest University PickAtlas	cerebellar gray matter	Huashan Hospital, Fudan University	2019.05- 2020.08
Liu et al. [124] 2023	NINCDS-ADRDA 2011 MDS 2017	SUVR	AAL3 MNI PD25 template	cerebellar gray matter	Huashan Hospital, Fudan University	2020.07- 2022.07
Messerschmidt et al. [125] 2022	MDS 2017	DVR	the atlas of the basal ganglia[6] The Brainnetom Atlas[7] Hammers	cerebellum (excluding the dentate nucleus and the central cerebellar white matter, as well as the superior and the posterior cerebellar layers)	Ludwig Maximilian University	NR
Ossenkoppele et al. [126] 2018	NINCDS-ADRDA 2011	SUVR	DK	the inferior cerebellar gray matter	(a) the Memory Disorder Clinic of Gangnam Severance Hospital	2014.09- 2017.11

Author. [ref] year	Reference Standard	Outcome	Atlas	Reference brain region	Source of data	Data range
	Jack CR Jr et al.[4]				(b) BioFINDER study (c) the University of California San Francisco Alzheimer Disease Research Center	
Palleis et al. [127] 2021	MDS 2017 the Armstrong criteria	DVR	Hammers	cerebellum (excluding dentate nucleus, superior and posterior layers)	Ludwig-Maximilians-University	NR
Schonhaut et al. [128] 2017	NINDS-SPSP 1996	SUVR	Talairach Atlas	cerebellar gray matter excluding dentate nucleus	(a)University of California San Francisco (b)University of California Berkeley (c)multicenter imaging trials sponsored by Avid Radiopharmaceuticals (d)Massachusetts General Hospital	NR
Song et al. [129] 2021	MDS 2017	DVR	Hammers ATAG atlases (the atlas of the Basal Ganglia)	cerebellum, excluding the dentate nucleus, the central cerebellar white matter, and the superior and the posterior cerebellar layers (d = 1.5 cm each)	five different specialized centers in three countries (Munich, PSP-RSd[Progressive supranuclear palsy-Richardson syndrome] n = 20; Leipzig, PSP-RS n = 11; Cologne, PSP-RS n = 2; New Haven, PSP-RS n = 4, HC n = 5; Melbourne, HC n = 5)	NR
Tagai et al. [130] 2021	NINCDS-ADRDA 1984 Petersen's criteria 1999 MDS 2017	SUVR	DK	cerebellar gray matter	National Institutes for Quantum and Radiological Science and Technology	NR
Zou et al. [131] 2021	NINCDS-ADRDA 2011	SUVR	Braak ROI	the inferior cerebellum	(a) Columbia University Irving Medical Center (b) ADNI	NR

SUVR standardized uptake value ratio, **DVR** distribution volume ratio, **BPND** binding potential, **DK** Desikan-Killiany-Tourville atlas, **AAL** anatomical automatic labeling, **NINCDS-ADRDA** National Institute of Neurological and Communicative Disorders and Stroke and the Alzheimer's Disease and Related Disorders Association, **APA** American Psychological Association, **MDS** Movement Disorder Society, **NINDS-SPSP** National Institute of Neurological Disorders

Author. [ref] year	Reference Standard	Outcome	Atlas	Reference brain region	Source of data	Data range

and Stroke and the Society for progressive supranuclear palsy, **CSF** cerebrospinal fluid, **CDR** clinical dementia rating, **NIA-AD** National Institute on Aging-Alzheimer's Disease, **MMSE** mini-mental state examination, **ROI** region-of-interest, **NR** not reported.

[1] Ilinsky I, Horn A, Paul-Gilloteaux P, et al. Human Motor Thalamus Reconstructed in 3D from Continuous Sagittal Sections with Identified Subcortical Afferent Territories. eNeuro 2018; 5: ENEURO.0060-18.2018.

[2] Höglinger GU, Respondek G, Stamelou M, et al. Clinical diagnosis of progressive supranuclear palsy: The movement disorder society criteria. Mov Disord Off J Mov Disord Soc 2017; 32: 853–864.

[3] Frazier JA, Chiu S, Breeze JL, et al. Structural brain magnetic resonance imaging of limbic and thalamic volumes in pediatric bipolar disorder. Am J Psychiatry 2005; 162: 1256–1265.

[4] Frazier JA, Chiu S, Breeze JL, et al. Structural brain magnetic resonance imaging of limbic and thalamic volumes in pediatric bipolar disorder. Am J Psychiatry 2005; 162: 1256–1265.

[5] Xiao Y, Fonov V, Chakravarty MM, et al. A dataset of multi-contrast population-averaged brain MRI atlases of a Parkinson□s disease cohort. Data Brief 2017; 12: 370–379.

[6] Keuken MC, Bazin P-L, Backhouse K, et al. Effects of aging on T_1, T_2*, and QSM MRI values in the subcortex. Brain Struct Funct 2017; 222: 2487–2505.

[7] Fan L, Li H, Zhuo J, et al. The Human Brainnetome Atlas: A New Brain Atlas Based on Connectional Architecture. Cereb Cortex N Y N 1991 2016; 26: 3508–3526.

The distribution of tau PET data across patient populations included AD versus HC (46 studies), PSP versus HCs (22 studies), CBS versus HCs (9 studies), and AD versus PSP (6 studies). Diagnostic performance data were available for differentiating AD patients from HCs (14 studies), PSP patients from HCs (7 studies), and AD/MCI patients from HCs (5 studies). Figures 2 and 3 and Supplementary Figs. 1–10 summarize the differences in tau tracer uptake among different tauopathies in different regions. The pooled performance of tau PET in the diagnosis of tauopathies is shown in Fig. 4 and Supplementary Figs. 11–15.

Brain region differences in tau tracer uptake between AD patients and HCs

Thirty brain regions were available for meta-analysis for comparisons between AD patients and HCs (Fig. 2). AD patients exhibited significantly elevated tau tracer uptake in 27 regions ($p < 0.01$), with the strongest effects observed in the lateral temporal (SMD = 2.58), Braak stage I/II regions (SMD = 2.40), and entorhinal cortex (SMD = 2.30). The SMD values ranged from 0.39 to 2.58, with regions listed in decreasing order based on effect size. Low between-study heterogeneity (I^2 = 0–48%) was observed in seven regions (amygdala, superior parietal, inferior parietal, superior temporal, orbitofrontal, and lingual gyri, and striatum), whereas the remaining regions exhibited moderate to high heterogeneity (I^2 range: 54–93%). No brain region showed significantly lower tau tracer uptake in AD patients than in HCs.

Eighteen brain regions classified by the type of study outcome were available for subgroup analysis (Supplementary Fig. 1). In the subgroup analysis, heterogeneity decreased in 58.8% of the regions (10/17) after excluding the amygdala (which initially showed low heterogeneity). DVR-based measurements revealed greater SMD values than SUVR in the frontal, parietal, and posterior cingulate gyri.

Subgroup analyses by atlas type revealed that compared with the Anatomical Automatic Labeling (AAL) atlas, the Desikan-Killiany (DK) atlas yielded significantly greater SMD values (mean difference = 0.39, p = 0.04). The heterogeneity decreased in 8/10 regions with the AAL atlas and 8/16 regions with the DK atlas after regions with initially low heterogeneity were excluded.

With respect to tracer type (Supplementary Fig. 3), [^{18}F]AV-1451 showed significantly elevated uptake in 12 brain regions in AD patients (SMD range: 0.87–2.69; $p < 0.01$), with heterogeneity decreasing across the eight regions. [^{18}F]FDDNP demonstrated increased binding in five brain regions (SMD range: 2.07–2.70; $p < 0.01$), with high heterogeneity persisting in most regions (I^2 range: 80–91%). [^{18}F]THK-5351 analysis revealed significantly higher uptake in the occipital (SMD = 1.50, $p < 0.01$) and fusiform gurus (SMD = 1.75, $p < 0.01$), with low heterogeneity (both $I^2 < 50\%$).

Brain region differences in tau tracer uptake between PSP patients and HCs

Our meta-analysis included 13 brain regions in PSP patients and HCs (Fig. 3). Eight regions showed significantly elevated tau tracer uptake in PSP patients ($p < 0.05$): the subthalamic nucleus (SMD = 1.71), globus pallidus (SMD = 1.43), red nucleus (SMD = 1.19), midbrain (SMD = 1.09), putamen (SMD = 0.77), dentate nucleus (SMD = 0.73), substantia nigra (SMD = 0.59), and parietal region (SMD = 0.41). Three regions demonstrated low heterogeneity (I^2=11–46%): the subthalamic nucleus, globus pallidus, and parietal region. The remaining regions showed moderate to high heterogeneity (I^2=50–80%). No brain region in patients with PSP presented significantly reduced tau tracer uptake compared with that in HCs.

Twelve brain regions underwent subgroup analysis by outcome type (Supplementary Fig. 5), revealing significantly increased tracer uptake in eight regions ($p < 0.05$). Notably, subgroup analysis revealed an elevated substantia nigra SMD above the dentate nucleus and significantly increased previously nonsignificant thalamic uptake (pre: SMD = 0.62, $p = 0.08$; post: SMD = 0.58, $p = 0.04$). (before: SMD = 0.62, $p = 0.08$; after: SMD = 0.58, $p = 0.04$). Conversely, the parietal region did not significantly differ after the subgroup analysis (before: SMD = 0.41, $p = 0.02$; after: SMD = 0.26, $p = 0.05$). Moreover, only the thalamus and parietal cortex exhibited reduced heterogeneity after subgrouping.

Two brain regions were available for atlas-based subgroup analysis (Supplementary Fig. 6). In studies using the AAL atlas, the heterogeneity of the putamen and globus pallidus markedly decreased ($I^2 = 0$ and 2, respectively). Only one brain region, the globus pallidus, could undergo subgroup analysis based on the DK atlas. The results indicated that heterogeneity remained low as the SMD decreased (SMD = 1.26, $I^2 = 47$).

With respect to tracer type (Supplementary Fig. 7), subgroup analyses revealed increased [18F]AV-1451 binding in the putamen ($p < 0.01$; heterogeneity reduced: I^2=50 to 18) and globus pallidus ($p < 0.01$) in PSP patients compared with HCs. [18F]PI-2620 exhibited elevated uptake in the dentate nucleus ($p < 0.01$), whereas subgroup analysis eliminated the difference in uptake in the substantia nigra (before: SMD = 0.59, $p < 0.01$; after: SMD = 0.39, $p = 0.08$), despite reduced heterogeneity (I^2=80 to 49). [18F] THK-5351 was associated with higher midbrain uptake in PSP patients (SMD = 1.43, $p = 0.02$), although the degree of heterogeneity remained high (I^2=81). [18F]PM-PBB3 demonstrated markedly increased subthalamic nucleus binding in PSP patients (SMD = 1.83, $p < 0.01$), with resolved heterogeneity (I^2=0).

Consistent findings were obtained for first- and second-generation tau tracers, with PSP patients exhibiting significantly higher uptake than HCs in all three assessable brain regions did (Supplementary Fig. 8). Paired t tests revealed no significant difference in the SMD values between the tracer groups (mean difference=-0.21; $p = 0.28$).

Brain region differences in tau tracer uptake between CBS patients and HCs

The tau uptake in four brain regions was elevated in CBS patients compared with HCs (precentral gyrus, globus pallidus, putamen, postcentral gyrus; SMD = 1.06–1.86; $p < 0.01$; Supplementary Fig. 9). Among these, only the postcentral gyrus exhibited low heterogeneity ($I^2 = 42$), whereas the other gyri presented high heterogeneity (I2 = 67–78). No regions exhibited reduced uptake. Subgroup analysis of the putamen retained significance (SMD = 1.31, $p < 0.01$) despite undiminished heterogeneity (I^2=70).

Brain region differences in tau tracer uptake between AD patients and PSP patients

Two brain regions were analyzed in AD patients and PSP patients (Supplementary Fig. 10). AD patients presented greater tau tracer uptake in the globus pallidus than did patients with PSP did (SMD=-1.47, $p < 0.01$; $I^2 = 9$), whereas the difference in the putamen was not significant (SMD=-0.61, $p = 0.21$).

Pooled performance of tau tracers for distinguishing AD patients from HCs

A total of 18 contingency tables from 14 studies on classifying AD patients from HCs were used. The overall pooled SE, SP, and AUC were 0.83 (95% CI: 0.76–0.89), 0.89 (95% CI: 0.85–0.92), and 0.92 (95% CI: 0.89–0.96), respectively. The heterogeneity for SE and SP was 81 and 60, respectively (Fig. 4). Individual hierarchical summary receiver SROC curves are shown in Supplementary Figs. 16–18.

With respect to the types of study outcomes, 16 contingency tables from 12 studies utilized the SUVR. The pooled SE, SP, and AUC were 0.85 (95% CI: 0.76–0.90), 0.89 (95% CI: 0.85–0.92), and 0.93 (95% CI: 0.89–0.96), respectively (Supplementary Fig. 11). The subgroup analysis did not reduce heterogeneity.

With respect to the atlas, 9 contingency tables from 6 studies utilized DK. The pooled SE and AUC were 0.92 (95% CI: 0.89–0.94), 0.91 (95% CI: 0.85–0.95), and 0.98 (95% CI: 0.96–0.99), respectively (Supplementary Fig. 12). Subgroup analysis revealed reduced heterogeneity in the SE in the DK group (I^2=32) but not in the SP group (I^2=72).

With respect to the tracer type, 6 contingency tables from 6 studies utilized [^{18}F]AV-1451 (Supplementary Fig. 13). The pooled SE, SP, and AUC were 0.81 (95% CI: 0.62–0.91), 0.91 (95% CI: 0.84–0.96), and 0.87 (95% CI: 0.79–0.96), respectively. Subgroup analysis reduced specificity heterogeneity (I^2=23) but not sensitivity (I^2=89).

First- and second-generation tau tracers (11 vs. 7 contingency tables; Fig. 4) demonstrated comparable pooled SEs (first-gen: 0.84, 95% CI: 0.73–0.91; second-gen: 0.83, 0.72–0.91) and SPs (first-gen: 0.88, 0.81–0.93; second-gen: 0.91, 0.86–0.94), with second-generation tracers showing superior AUCs (0.98, 0.97–0.99 vs. 0.89, 0.84–0.94). Subgroup analysis revealed minimal variation in SE and SP for both groups.

Pooled performance of the tau tracer for distinguishing PSP patients from HCs

Seven contingency tables from 7 studies on classifying PSP patients from HCs were constructed (Supplementary Fig. 14). The overall pooled SE, SP, and AUC were 0.88 (95% CI: 0.83–0.92), 0.93 (95% CI: 0.87–0.96), and 0.92 (95% CI: 0.85–0.99), respectively.

Pooled performance of tau tracers for distinguishing AD/MCI patients from HCs

Seven contingency tables from 5 studies on the classification of AD/MCI patients from HCs were constructed (Supplementary Fig. 15). The overall pooled SE, SP, and AUC were 0.75 (95% CI: 0.48–0.91), 0.97 (95% CI: 0.92–0.99), and 0.84 (95% CI: 0.74–0.94), respectively.

Discussion

The advent of tau PET molecular imaging has revolutionized the in vivo characterization of tauopathies by enabling the precise mapping of tau aggregates and enhancing diagnostic accuracy. This meta-analysis of 80 studies (n = 9,166)

provides the most comprehensive synthesis to date, yielding two key findings: (1) disease-specific spatial patterns of tau deposition align with established neuropathological staging systems and (2) high diagnostic accuracy of tau PET in differentiating between patients with tauopathies and healthy controls. While these findings demonstrate the significant potential of tau PET in clinical diagnosis, our analysis also revealed important methodological limitations that must be addressed for optimal clinical application.

In AD, tau PET deposition mirrors postmortem Braak staging, with the strongest effects in the Braak I-II regions (SMD = 2.40, 95% CI: 1.75–3.06), notably peaking in the entorhinal cortex (SMD = 2.30), followed by the Braak III-IV limbic areas (SMD = 2.26, 95% CI: 1.64–2.87) and the Braak V-VI neocortical regions (SMD = 2.08, 95% CI: 1.54–2.63), thereby substantiating transsynaptic propagation in vivo [21]. Our analyses also revealed accelerated neocortical tau propagation, as evidenced by increased tau burden in the lateral versus the medial temporal lobes (SMD = 2.58 vs. 1.75; $p < 0.001$). Neuroimaging trajectories further demonstrated that the precuneus exhibited a 2.7-fold faster annual tau accumulation rate than the entorhinal cortex did (ΔSUVR: 0.16 ± 0.18 vs. 0.03 ± 0.07; p = 0.04) [22], suggesting a threshold-dependent transition from limbic to neocortical tau spread, potentially indicating the onset of rapid clinical deterioration near symptom emergence. Clinically, Aβ PET remains the earliest detectable AD biomarker and predicts downstream tauopathy with > 90% specificity for intermediate/high neuropathologic change [23]. However, amyloid positivity can precede symptoms by up to two decades, limiting its prognostic usefulness [24–26]. In contrast, tau PET is strongly correlated with disease severity and clinical decline and outperforms Aβ PET in predicting dementia progression [27–29]. Protective Apolipoprotein3 Christchurch homozygotes, who resist cognitive decline despite heavy amyloidosis, suggest that tau, not amyloid, drives neurodegeneration through propagation and glial activation [30, 31]. These findings position tau PET as a superior tool for both early staging and prognosis in AD, suggesting that therapeutic trials should prioritize tau burden as a primary endpoint [32, 33]. However, the absence of regions with reduced tau tracer uptake in AD undermines compensatory synaptic remodeling [34], and deeper mechanistic studies are needed.

Consistent with prior reports that tau PET differentiates AD patients from HCs more robustly than 3R and 4R tauopathies do [16, 35], we observed significant tau elevations in eight regions in PSP patients ($p < 0.05$) versus 27 in AD patients ($p < 0.01$). In PSP, tracer uptake was concentrated in subcortical motor circuits: the subthalamic nucleus (SMD = 1.71, 95% CI: 1.49–1.93) and globus pallidus (SMD = 1.43, 95% CI: 1.18–1.69) showed the greatest effects, which is consistent with basal ganglia-thalamo-cortical involvement [36, 37]. The subthalamic nucleus exhibited low heterogeneity (I^2=11%), whereas midbrain regions displayed high heterogeneity (I^2=73–80%), likely reflecting off-target binding of [^{18}F]AV-1451 [12]. These findings underscore the necessity of 4R-tau-selective ligands for accurate PSP evaluation.

Our study revealed significantly higher globus pallidus tau tracer uptake in AD patients than in PSP patients (SMD=-1.47, $p < 0.01$; I^2=9%), reflecting divergent tau pathology and connectivity. In AD, neurofibrillary tangles (NFTs) composed of mixed 3R/4R tau isoforms predominantly accumulate in neurons [38], which spread from limbic regions to basal ganglia structures such as the globus pallidus—a key hub in limbic–striatal circuits vulnerable to transsynaptic tau propagation [39]. Conversely, PSP pathology is characterized by 4R-tau aggregates localized in astrocytes and oligodendrocytes [40] but relatively sparing the neuron-rich globus pallidus [41]. Notably, sparse astrocytic inclusions and partial-volume effects further diminish the PET signal in PSP [42]. These distinctions underscore the urgent need to characterize tracer affinities for 3R versus 4R isoforms and for neuronal versus glial tau to increase diagnostic specificity.

Tau PET shows robust diagnostic accuracy across tauopathies. In AD, second-generation tracers outperform first-generation agents (AUC 0.98 vs. 0.89; $p < 0.001$), likely because of improved 3R/4R selectivity and reduced off-target binding. Standardized protocols utilizing the DK atlas further optimized accuracy (AUC = 0.98 vs. 0.92). With respect to PSP, tau PET achieved an SE of 0.88 and SP of 0.93, whereas for MCI due to AD, the SP remained high (0.97), but the SE decreased to 0.75, reflecting cohort heterogeneity and early pathological thresholds. Notably, recent validation studies revealed that the temporal meta-ROI quantification and visual reads each reached an AUC of 0.85 ($p < 0.05$) for predicting MCI-to-AD conversion [29], indicating that region-specific approaches can partially offset reduced SE. These results

underscore the value of integrating tau PET with complementary biomarkers and standardized protocols to improve early detection in preclinical and prodromal stages.

Methodological heterogeneity across tau PET studies, stemming from divergent acquisition protocols, processing pipelines, ROI definitions, and spatial normalization templates (e.g., AAL vs. DK), undermines comparability and Braak-region alignment. Inconsistent choice of reference regions (cerebellar gray matter vs. eroded white matter or composites) adds further variability [43, 44]. Although the universal “CenTauR” scale seeks to harmonize multitracer quantification, its validation is limited by tracer-specific differences and incomplete neuropathological calibration [45, 46]. Future work must prioritize inclusive tracer harmonization, neuropathology-anchored scaling, and autopsy-verified thresholds to minimize variability and ensure reproducible, multicenter applicability.

To facilitate clinical translation, we propose a three-pillar standardization framework: (1) harmonized acquisition using tracer-specific dynamic protocols or consensus static windows validated against kinetic models; (2) consistent processing via unified pipelines (e.g., MNI/ANTs) and histopathology-anchored reference regions; and (3) ROI harmonization through data-driven, Braak stage-specific parcellations from longitudinal cohorts. While artificial intelligence-driven analytics offer quantitative precision [47–49], they remain limited by data transparency and validation deficits [50], and visual reads, although subjective, retain clinical value. Therefore, integrating harmonized acquisition, robust computation, and expert interpretation will facilitate a multimodal, precision-medicine approach to tauopathy diagnostics and accelerate multicenter implementation.

Current tauopathy research faces additional challenges stemming from the clinicopathological characteristics and underrepresentation of rare entities. CBS, a syndrome rather than a single entity, comprises diverse pathologies—CBD (32%), PSP (31%), AD (20%), and others (17% [4]—leading to confounded comparisons with prototypical AD or PSP cohorts. Our meta-analysis confirmed predominant tau accumulation in motor-related cortical (pre/postcentral gyri) and subcortical (putamen, globus pallidus) regions but with substantial heterogeneity (I^2=42–78%). Additionally, autopsy studies revealed clinical-pathological discordance in more than 65% of CBS patients, only 35% of whom had true CBD [51]. Moreover, entities such as CTE and PiD are underpowered (fewer than five quantitative studies), risking type II error and bias [52]. To address these gaps, three strategic priorities emerge: (1) pathologically anchored prospective cohorts using the ATN framework to reduce misclassification [53]; (2) harmonized, multiscale data integration from deep phenotyping to standardized postmortem protocols; and (3) data-driven, head-to-head comparisons across tauopathies to refine disease taxonomy and enhance mechanistic insights.

This study has several limitations. First, the exclusive focus on English-language publications introduces potential selection bias, as non-English literature was systematically excluded. Second, to maintain methodological consistency, we did not contact the authors of studies with insufficiently reported data. Third, methodological heterogeneity across studies, in terms of imaging protocols, clinical validation criteria, and population characteristics—presents challenges for direct comparisons despite our subgroup analysis. Fourth, the limited availability of pathologically confirmed tauopathy diagnoses raises concerns about misclassification bias, as clinical criteria alone may not reliably distinguish between tauopathies. These limitations underscore the need for homogeneous, pathologically confirmed cohorts and transparent data-sharing practices to optimize the diagnostic utility of tau PET.

Conclusion

Our findings highlight the transformative potential of tau PET in detecting tauopathies. The technique demonstrates disease-specific topographic patterns that align with neuropathological staging and provides high diagnostic accuracy, particularly when second-generation tracers and standardized protocols are used. Future advancements should focus on standardized imaging methodologies, longitudinal validation with neuropathological correlation, and the development of

tracers with enhanced isoform specificity. These improvements ultimately support the development of personalized therapeutic strategies for tau-associated neurodegenerative disorders.

Declarations

Funding This study was funded by the National Natural Science Foundation of China [grants

No. 82272039, 82021002, and 82394434], and STI2030-Major Projects [grants No.

2022ZD0211606].

Competing interests The authors have no relevant financial or nonfinancial interests to disclose.

Author contributions Q.J. and J.W. contributed equally to this work. C.Z., R.N. and J.W. contributed to the conception and design of the study. Q.J., J.W., J.G. and Y.L. contributed to the literature search and data extraction. Q.J., H.L. and B.Y. contributed to the risk of bias evaluation. Q.J. and J.W. contributed to the data analysis and interpretation. Q.J. and J.W. drafted the initial manuscript. C.Z., R.N. and J.L. revised the

manuscript. C.Z. and R.N. was responsible for the decision to submit the manuscript. All authors have made important intellectual contributions and have seen and approved the final version of the manuscript for submission.

Data availability The authors declare that all the data included in this study are available within the paper and its Supplementary Information files.

Ethical approval Ethical approval was not needed, as this study was a systematic review and meta-analysis.

Consent to participate Informed consent was not necessary, as this study did not include any human experiments.

Consent to publish The study does not contain any individual person’s data in any form (including any individual details, images or videos).

References

1. Avila J, Lucas JJ, Perez M, et al. Role of tau protein in both physiological and pathological conditions. Physiol Rev. 2004;84:361–84.
2. Stancu I-C, Vasconcelos B, Ris L, et al. Templated misfolding of Tau by prion-like seeding along neuronal connections impairs neuronal network function and associated behavioral outcomes in Tau transgenic mice. Acta Neuropathol (Berl). 2015;129:875–94.
3. Chung D-EC, Roemer S, Petrucelli L, et al. Cellular and pathological heterogeneity of primary tauopathies. Mol Neurodegener. 2021;16:57.
4. Koga S, Josephs KA, Aiba I, et al. Neuropathology and emerging biomarkers in corticobasal syndrome. J Neurol Neurosurg Psychiatry. 2022;93:919–29.
5. Kovacs GG. Invited review: Neuropathology of tauopathies: principles and practice. Neuropathol Appl Neurobiol. 2015;41:3–23.
6. Warren NM, Piggott MA, Perry EK, et al. Cholinergic systems in progressive supranuclear palsy. Brain J Neurol. 2005;128:239–49.
7. Jack CR, Bennett DA, Blennow K, et al. NIA-AA Research Framework: Toward a biological definition of Alzheimer’s disease. Alzheimers Dement J Alzheimers Assoc. 2018;14:535–62.

8. Shulman M, Kong J, O'Gorman J, et al. TANGO: a placebo-controlled randomized phase 2 study of efficacy and safety of the anti-tau monoclonal antibody gosuranemab in early Alzheimer's disease. Nat Aging. 2023;3:1591–601.
9. Novak P, Schmidt R, Kontsekova E, et al. Safety and immunogenicity of the tau vaccine AADvac1 in patients with Alzheimer's disease: a randomised, double-blind, placebo-controlled, phase 1 trial. Lancet Neurol. 2017;16:123–34.
10. Höglinger GU, Huppertz H-J, Wagenpfeil S, et al. Tideglusib reduces progression of brain atrophy in progressive supranuclear palsy in a randomized trial. Mov Disord Off J Mov Disord Soc. 2014;29:479–87.
11. Leuzy A, Chiotis K, Lemoine L, et al. Tau PET imaging in neurodegenerative tauopathies-still a challenge. Mol Psychiatry. 2019;24:1112–34.
12. Yap SY, Frias B, Wren MC, et al. Discriminatory ability of next-generation tau PET tracers for Alzheimer's disease. Brain J Neurol. 2021;144:2284–90.
13. Groot C, Villeneuve S, Smith R, et al. Tau PET Imaging in Neurodegenerative Disorders. J Nucl Med Off Publ Soc Nucl Med. 2022;63:S20–6.
14. Wang YT, Edison P. Tau Imaging in Neurodegenerative Diseases Using Positron Emission Tomography. Curr Neurol Neurosci Rep. 2019;19:45.
15. Brendel M, Barthel H, van Eimeren T, et al. Assessment of 18F-PI-2620 as a Biomarker in Progressive Supranuclear Palsy. JAMA Neurol. 2020;77:1408–19.
16. Passamonti L, Vázquez Rodríguez P, Hong YT, et al. 18F-AV-1451 positron emission tomography in Alzheimer's disease and progressive supranuclear palsy. Brain J Neurol. 2017;140:781–91.
17. Whiting PF, Rutjes AWS, Westwood ME, et al. QUADAS-2: a revised tool for the quality assessment of diagnostic accuracy studies. Ann Intern Med. 2011;155:529–36.
18. Stang A. Critical evaluation of the Newcastle-Ottawa scale for the assessment of the quality of nonrandomized studies in meta-analyses. Eur J Epidemiol. 2010;25:603–5.
19. Higgins JPT, Thompson SG, Deeks JJ, et al. Measuring inconsistency in meta-analyses. BMJ. 2003;327:557–60.
20. Jackson D, Turner R. Power analysis for random-effects meta-analysis. Res Synth Methods. 2017;8:290–302.
21. Braak H, Del Tredici K. The pathological process underlying Alzheimer's disease in individuals under thirty. Acta Neuropathol (Berl). 2011;121:171–81.
22. Sanchez JS, Hanseeuw BJ, Lopera F, et al. Longitudinal amyloid and tau accumulation in autosomal dominant Alzheimer's disease: findings from the Colombia-Boston (COLBOS) biomarker study. Alzheimers Res Ther. 2021;13:27.
23. Jack CR, Andrews JS, Beach TG, et al. Revised criteria for diagnosis and staging of Alzheimer's disease: Alzheimer's Association Workgroup. Alzheimers Dement J Alzheimers Assoc. 2024;20:5143–69.
24. Jack CR, Knopman DS, Jagust WJ, et al. Tracking pathophysiological processes in Alzheimer's disease: an updated hypothetical model of dynamic biomarkers. Lancet Neurol. 2013;12:207–16.
25. Jansen WJ, Ossenkoppele R, Knol DL, et al. Prevalence of cerebral amyloid pathology in persons without dementia: a meta-analysis. JAMA. 2015;313:1924–38.
26. Caselli RJ, Langlais BT, Dueck AC, et al. Neuropsychological decline up to 20 years before incident mild cognitive impairment. Alzheimers Dement J Alzheimers Assoc. 2020;16:512–23.
27. Ossenkoppele R, Schonhaut DR, Schöll M, et al. Tau PET patterns mirror clinical and neuroanatomical variability in Alzheimer's disease. Brain J Neurol. 2016;139:1551–67.
28. Schwarz AJ, Yu P, Miller BB, et al. Regional profiles of the candidate tau PET ligand 18F-AV-1451 recapitulate key features of Braak histopathological stages. Brain J Neurol. 2016;139:1539–50.
29. Groot C, Smith R, Collij LE, et al. Tau Positron Emission Tomography for Predicting Dementia in Individuals With Mild Cognitive Impairment. JAMA Neurol. 2024;81:845–56.

30. Sepulveda-Falla D, Sanchez JS, Almeida MC, et al. Distinct tau neuropathology and cellular profiles of an APOE3 Christchurch homozygote protected against autosomal dominant Alzheimer's dementia. Acta Neuropathol (Berl). 2022;144:589–601.
31. Arboleda-Velasquez JF, Lopera F, O'Hare M, et al. Resistance to autosomal dominant Alzheimer's disease in an APOE3 Christchurch homozygote: a case report. Nat Med. 2019;25:1680–3.
32. Teng E, Manser PT, Pickthorn K, et al. Safety and Efficacy of Semorinemab in Individuals With Prodromal to Mild Alzheimer Disease: A Randomized Clinical Trial. JAMA Neurol. 2022;79:758–67.
33. Congdon EE, Ji C, Tetlow AM, et al. Tau-targeting therapies for Alzheimer disease: current status and future directions. Nat Rev Neurol. 2023;19:715–36.
34. Torrealba E, Aguilar-Zerpa N, Garcia-Morales P et al. Compensatory Mechanisms in Early Alzheimer's Disease and Clinical Setting: The Need for Novel Neuropsychological Strategies. J Alzheimers Dis Rep; 7: 513–25.
35. Smith R, Schöll M, Widner H, et al. In vivo retention of 18F-AV-1451 in corticobasal syndrome. Neurology. 2017;89:845–53.
36. Foster NN, Barry J, Korobkova L, et al. The mouse cortico-basal ganglia-thalamic network. Nature. 2021;598:188–94.
37. Dickson DW, Rademakers R, Hutton ML. Progressive supranuclear palsy: pathology and genetics. Brain Pathol Zurich Switz. 2007;17:74–82.
38. Narasimhan S, Changolkar L, Riddle DM, et al. Human tau pathology transmits glial tau aggregates in the absence of neuronal tau. J Exp Med. 2020;217:e20190783.
39. de Calignon A, Polydoro M, Suárez-Calvet M, et al. Propagation of tau pathology in a model of early Alzheimer's disease. Neuron. 2012;73:685–97.
40. Narasimhan S, Guo JL, Changolkar L, et al. Pathological Tau Strains from Human Brains Recapitulate the Diversity of Tauopathies in Nontransgenic Mouse Brain. J Neurosci Off J Soc Neurosci. 2017;37:11406–23.
41. Williams DR, Lees AJ. Progressive supranuclear palsy: clinicopathological concepts and diagnostic challenges. Lancet Neurol. 2009;8:270–9.
42. Slemann L, Gnörich J, Hummel S, et al. Neuronal and oligodendroglial, but not astroglial, tau translates to in vivo tau PET signals in individuals with primary tauopathies. Acta Neuropathol (Berl). 2024;148:70.
43. Schöll M, Lockhart SN, Schonhaut DR, et al. PET Imaging of Tau Deposition in the Aging Human Brain. Neuron. 2016;89:971–82.
44. Young CB, Landau SM, Harrison TM, et al. Influence of common reference regions on regional tau patterns in cross-sectional and longitudinal [18F]-AV-1451 PET data. NeuroImage. 2021;243:118553.
45. Leuzy A, Raket LL, Villemagne VL, et al. Harmonizing tau positron emission tomography in Alzheimer's disease: The CenTauR scale and the joint propagation model. Alzheimers Dement J Alzheimers Assoc. 2024;20:5833–48.
46. Villemagne VL, Leuzy A, Bohorquez SS, et al. CenTauR: Toward a universal scale and masks for standardizing tau imaging studies. Alzheimers Dement Amst Neth. 2023;15:e12454.
47. Moradi E, Prakash M, Hall A, et al. Machine learning prediction of future amyloid beta positivity in amyloid-negative individuals. Alzheimers Res Ther. 2024;16:46.
48. Gebre RK, Rial AM, Raghavan S, et al. Advancing Tau PET Quantification in Alzheimer Disease with Machine Learning: Introducing THETA, a Novel Tau Summary Measure. J Nucl Med Off Publ Soc Nucl Med. 2024;65:1473–80.
49. Chen K, Weng Y, Hosseini AA, et al. A comparative study of GNN and MLP based machine learning for the diagnosis of Alzheimer's Disease involving data synthesis. Neural Netw Off J Int Neural Netw Soc. 2024;169:442–52.
50. Wang J, Xue L, Jiang J, et al. Diagnostic performance of artificial intelligence-assisted PET imaging for Parkinson's disease: a systematic review and meta-analysis. NPJ Digit Med. 2024;7:17.

51. Lee SE, Rabinovici GD, Mayo MC, et al. Clinicopathological correlations in corticobasal degeneration. Ann Neurol. 2011;70:327–40.
52. Debray TPA, Moons KGM, Riley RD. Detecting small-study effects and funnel plot asymmetry in meta-analysis of survival data: A comparison of new and existing tests. Res Synth Methods. 2018;9:41–50.
53. Cheng Y, Chen S-F, Zhang Y-R, et al. Novel diagnostic and prognostic approach for rapidly progressive dementias: Indicators based on amyloid/tau/neurodegeneration (ATN) framework. CNS Neurosci Ther. 2024;30:e14857.
54. Baker SL, Lockhart SN, Price JC, et al. Reference Tissue-Based Kinetic Evaluation of 18F-AV-1451 for Tau Imaging. J Nucl Med Off Publ Soc Nucl Med. 2017;58:332–8.
55. Barret O, Alagille D, Sanabria S, et al. Kinetic Modeling of the Tau PET Tracer 18F-AV-1451 in Human Healthy Volunteers and Alzheimer Disease Subjects. J Nucl Med Off Publ Soc Nucl Med. 2017;58:1124–31.
56. Barrio JR, Small GW, Wong K-P, et al. In vivo characterization of chronic traumatic encephalopathy using [F-18]FDDNP PET brain imaging. Proc Natl Acad Sci U S A. 2015;112:E2039–2047.
57. Barthélemy NR, Toth B, Manser PT, et al. Site-Specific Cerebrospinal Fluid Tau Hyperphosphorylation in Response to Alzheimer's Disease Brain Pathology: Not All Tau Phospho-Sites are Hyperphosphorylated. J Alzheimers Dis JAD. 2022;85:415–29.
58. Blazhenets G, Soleimani-Meigooni DN, Thomas W, et al. [18F]PI-2620 Binding Patterns in Patients with Suspected Alzheimer Disease and Frontotemporal Lobar Degeneration. J Nucl Med Off Publ Soc Nucl Med. 2023;64:1980–9.
59. Brendel M, Schönecker S, Höglinger G, et al. [18F]-THK5351 PET Correlates with Topology and Symptom Severity in Progressive Supranuclear Palsy. Front Aging Neurosci. 2017;9:440.
60. Bun S, Moriguchi S, Tezuka T, et al. Findings of 18 F-PI-2620 tau PET imaging in patients with Alzheimer's disease and healthy controls in relation to the plasma P-tau181 levels in a Japanese sample. Neuropsychopharmacol Rep. 2022;42:437–48.
61. Chen ST, Siddarth P, Merrill DA, et al. FDDNP-PET Tau Brain Protein Binding Patterns in Military Personnel with Suspected Chronic Traumatic Encephalopathy1. J Alzheimers Dis JAD. 2018;65:79–88.
62. Cho H, Choi JY, Hwang MS, et al. Tau PET in Alzheimer disease and mild cognitive impairment. Neurology. 2016;87:375–83.
63. Cho H, Choi JY, Hwang MS, et al. Subcortical 18 F-AV-1451 binding patterns in progressive supranuclear palsy. Mov Disord Off J Mov Disord Soc. 2017;32:134–40.
64. Cho H, Choi JY, Lee SH, et al. Excessive tau accumulation in the parieto-occipital cortex characterizes early-onset Alzheimer's disease. Neurobiol Aging. 2017;53:103–11.
65. Coakeley S, Cho SS, Koshimori Y, et al. Positron emission tomography imaging of tau pathology in progressive supranuclear palsy. J Cereb Blood Flow Metab Off J Int Soc Cereb Blood Flow Metab. 2017;37:3150–60.
66. Ezura M, Kikuchi A, Okamura N, et al. 18F-THK5351 Positron Emission Tomography Imaging in Neurodegenerative Tauopathies. Front Aging Neurosci. 2021;13:761010.
67. Gonzalez C, Tommasi NS, Briggs D, et al. Financial Capacity and Regional Cerebral Tau in Cognitively Normal Older Adults, Mild Cognitive Impairment, and Alzheimer's Disease Dementia. J Alzheimers Dis JAD. 2021;79:1133–42.
68. Harada R, Okamura N, Furumoto S, et al. [(18)F]THK-5117 PET for assessing neurofibrillary pathology in Alzheimer's disease. Eur J Nucl Med Mol Imaging. 2015;42:1052–61.
69. Harrison TM, La Joie R, Maass A, et al. Longitudinal tau accumulation and atrophy in aging and alzheimer disease. Ann Neurol. 2019;85:229–40.
70. Hsu J-L, Chen S-H, Hsiao I-T, et al. 18F-THK5351 PET imaging in patients with progressive supranuclear palsy: associations with core domains and diagnostic certainty. Sci Rep. 2020;10:19410.
71. Hsu J-L, Lin K-J, Hsiao I-T, et al. The Imaging Features and Clinical Associations of a Novel Tau PET Tracer-18F-APN1607 in Alzheimer Disease. Clin Nucl Med. 2020;45:747–56.

72. Ishiki A, Harada R, Okamura N, et al. Tau imaging with [18 F]THK-5351 in progressive supranuclear palsy. Eur J Neurol. 2017;24:130–6.
73. Jantarato A, Vachatimanont S, Boonkawin N et al. The Evaluation of Tau Deposition with [18F]PI-2620 by Using a Semiquantitative Method in Cognitively Normal Subjects and Patients with Mild Cognitive Impairment and Alzheimer's Disease. Mol Imaging. 2021; 2021: 6640054.
74. Jeon S, Kang JM, Seo S, et al. Topographical Heterogeneity of Alzheimer's Disease Based on MR Imaging, Tau PET, and Amyloid PET. Front Aging Neurosci. 2019;11:211.
75. Johnson KA, Schultz A, Betensky RA, et al. Tau positron emission tomographic imaging in aging and early Alzheimer disease. Ann Neurol. 2016;79:110–9.
76. Kang JM, Lee S-Y, Seo S, et al. Tau positron emission tomography using [18F]THK5351 and cerebral glucose hypometabolism in Alzheimer's disease. Neurobiol Aging. 2017;59:210–9.
77. Kepe V, Bordelon Y, Boxer A, et al. PET imaging of neuropathology in tauopathies: progressive supranuclear palsy. J Alzheimers Dis JAD. 2013;36:145–53.
78. Kikuchi A, Okamura N, Hasegawa T, et al. In vivo visualization of tau deposits in corticobasal syndrome by 18F-THK5351 PET. Neurology. 2016;87:2309–16.
79. Krishnadas N, Doré V, Robertson JS, et al. Rates of regional tau accumulation in ageing and across the Alzheimer's disease continuum: an AIBL 18F-MK6240 PET study. EBioMedicine. 2023;88:104450.
80. Lagarde J, Olivieri P, Caillé F, et al. [18F]-AV-1451 tau PET imaging in Alzheimer's disease and suspected non-AD tauopathies using a late acquisition time window. J Neurol. 2019;266:3087–97.
81. Lagarde J, Olivieri P, Tonietto M, et al. Tau-PET imaging predicts cognitive decline and brain atrophy progression in early Alzheimer's disease. J Neurol Neurosurg Psychiatry. 2022;93:459–67.
82. Lee SH, Cho H, Choi JY, et al. Distinct patterns of amyloid-dependent tau accumulation in Lewy body diseases. Mov Disord Off J Mov Disord Soc. 2018;33:262–72.
83. Li C-H, Chen T-F, Chiu M-J, et al. Integrated 18F-T807 Tau PET, Structural MRI, and Plasma Tau in Tauopathy Neurodegenerative Disorders. Front Aging Neurosci. 2021;13:646440.
84. Liu F-T, Lu J-Y, Li X-Y, et al. 18F-Florzolotau PET imaging captures the distribution patterns and regional vulnerability of tau pathology in progressive supranuclear palsy. Eur J Nucl Med Mol Imaging. 2023;50:1395–405.
85. Lu J, Bao W, Li M, et al. Associations of [18F]-APN-1607 Tau PET Binding in the Brain of Alzheimer's Disease Patients With Cognition and Glucose Metabolism. Front Neurosci. 2020;14:604.
86. Meindl M, Zatcepin A, Gnörich J, et al. Assessment of [18F]PI-2620 Tau-PET Quantification via Non-Invasive Automatized Image Derived Input Function. Eur J Nucl Med Mol Imaging. 2024;51:3252–66.
87. Mueller A, Bullich S, Barret O, et al. Tau PET imaging with 18F-PI-2620 in Patients with Alzheimer Disease and Healthy Controls: A First-in-Humans Study. J Nucl Med Off Publ Soc Nucl Med. 2020;61:911–9.
88. Nam G, Jeong HJ, Kang JM, et al. 18F-THK5351 PET Imaging in the Behavioral Variant of Frontotemporal Dementia. Dement Neurocognitive Disord. 2018;17:163–73.
89. Ng KP, Therriault J, Kang MS, et al. Rasagiline, a monoamine oxidase B inhibitor, reduces in vivo [18F]THK5351 uptake in progressive supranuclear palsy. NeuroImage Clin. 2019;24:102091.
90. Niccolini F, Wilson H, Hirschbichler S, et al. Disease-related patterns of in vivo pathology in Corticobasal syndrome. Eur J Nucl Med Mol Imaging. 2018;45:2413–25.
91. Nihashi T, Sakurai K, Kato T, et al. Patterns of Distribution of 18F-THK5351 Positron Emission Tomography in Alzheimer's Disease Continuum. J Alzheimers Dis JAD. 2022;85:223–34.
92. Okamura N, Furumoto S, Fodero-Tavoletti MT, et al. Non-invasive assessment of Alzheimer's disease neurofibrillary pathology using 18F-THK5105 PET. Brain J Neurol. 2014;137:1762–71.

93. Oliveira Hauer K, Pawlik D, Leuzy A, et al. Performance of [18F]RO948 PET, MRI and CSF neurofilament light in the differential diagnosis of progressive supranuclear palsy. Parkinsonism Relat Disord. 2023;106:105226.
94. Pascoal TA, Therriault J, Benedet AL, et al. 18F-MK-6240 PET for early and late detection of neurofibrillary tangles. Brain J Neurol. 2020;143:2818–30.
95. Santillo AF, Leuzy A, Honer M, et al. [18F]RO948 tau positron emission tomography in genetic and sporadic frontotemporal dementia syndromes. Eur J Nucl Med Mol Imaging. 2023;50:1371–83.
96. Small GW, Kepe V, Ercoli LM, et al. PET of brain amyloid and tau in mild cognitive impairment. N Engl J Med. 2006;355:2652–63.
97. Smith R, Schain M, Nilsson C, et al. Increased basal ganglia binding of 18 F-AV-1451 in patients with progressive supranuclear palsy. Mov Disord Off J Mov Disord Soc. 2017;32:108–14.
98. Tagai K, Ikoma Y, Endo H et al. NeuroImage. An optimized reference tissue method for quantification of tau protein depositions in diverse neurodegenerative disorders by PET with 18F-PM-PBB3 (18F-APN-1607). 2022; 264: 119763.
99. Tauber C, Beaufils E, Hommet C, et al. Brain [18F]FDDNP binding and glucose metabolism in advanced elderly healthy subjects and Alzheimer's disease patients. J Alzheimers Dis JAD. 2013;36:311–20.
100. Tolboom N, Yaqub M, van der Flier WM, et al. Detection of Alzheimer pathology in vivo using both 11C-PIB and 18F-FDDNP PET. J Nucl Med Off Publ Soc Nucl Med. 2009;50:191–7.
101. Tsai RM, Bejanin A, Lesman-Segev O, et al. 18F-flortaucipir (AV-1451) tau PET in frontotemporal dementia syndromes. Alzheimers Res Ther. 2019;11:13.
102. Villemagne VL, Furumoto S, Fodero-Tavoletti MT, et al. In vivo evaluation of a novel tau imaging tracer for Alzheimer's disease. Eur J Nucl Med Mol Imaging. 2014;41:816–26.
103. Wardak M, Wong K-P, Shao W, et al. Movement correction method for human brain PET images: application to quantitative analysis of dynamic 18F-FDDNP scans. J Nucl Med Off Publ Soc Nucl Med. 2010;51:210–8.
104. Wolters EE, van de Beek M, Ossenkoppele R, et al. Tau PET and relative cerebral blood flow in dementia with Lewy bodies: A PET study. NeuroImage Clin. 2020;28:102504.
105. Wong DF, Comley RA, Kuwabara H, et al. Characterization of 3 Novel Tau Radiopharmaceuticals, 11C-RO-963, 11C-RO-643, and 18F-RO-948, in Healthy Controls and in Alzheimer Subjects. J Nucl Med Off Publ Soc Nucl Med. 2018;59:1869–76.
106. Yoon CW, Jeong HJ, Seo S, et al. 18F-THK5351 PET Imaging in Nonfluent-Agrammatic Variant Primary Progressive Aphasia. Dement Neurocognitive Disord. 2018;17:110–9.
107. Dang M, Chen Q, Zhao X, et al. Tau as a biomarker of cognitive impairment and neuropsychiatric symptom in Alzheimer's disease. Hum Brain Mapp. 2023;44:327–40.
108. Jiao F, Wang M, Sun X, et al. Based on Tau PET Radiomics Analysis for the Classification of Alzheimer's Disease and Mild Cognitive Impairment. Brain Sci. 2023;13:367.
109. Lin H-C, Lin K-J, Huang K-L, et al. Visual reading for [18F]Florzolotau ([18F]APN-1607) tau PET imaging in clinical assessment of Alzheimer's disease. Front Neurosci. 2023;17:1148054.
110. Maass A, Landau S, Baker SL, et al. Comparison of multiple tau-PET measures as biomarkers in aging and Alzheimer's disease. NeuroImage. 2017;157:448–63.
111. Mattsson N, Smith R, Strandberg O, et al. Comparing 18F-AV-1451 with CSF t-tau and p-tau for diagnosis of Alzheimer disease. Neurology. 2018;90:e388–95.
112. Rullmann M, Brendel M, Schroeter ML, et al. Multicenter 18F-PI-2620 PET for In Vivo Braak Staging of Tau Pathology in Alzheimer's Disease. Biomolecules. 2022;12:458.
113. Seibyl JP, DuBois JM, Racine A, et al. A Visual Interpretation Algorithm for Assessing Brain Tauopathy with 18F-MK-6240 PET. J Nucl Med Off Publ Soc Nucl Med. 2023;64:444–51.

114. Tolboom N, van der Flier WM, Boverhoff J, et al. Molecular imaging in the diagnosis of Alzheimer's disease: visual assessment of [11C]PIB and [18F]FDDNP PET images. J Neurol Neurosurg Psychiatry. 2010;81:882–4.
115. Yokoi T, Watanabe H, Yamaguchi H, et al. Involvement of the Precuneus/Posterior Cingulate Cortex Is Significant for the Development of Alzheimer's Disease: A PET (THK5351, PiB) and Resting fMRI Study. Front Aging Neurosci. 2018;10:304.
116. Chanisa C, Monchaya N, Anchisa K, et al. Analysis of amyloid and tau deposition in Alzheimer's disease using 11C-Pittsburgh compound B and 18F-THK 5351 positron emission tomography imaging. World J Nucl Med. 2021;20:61–72.
117. Chen J, Li Y, Pirraglia E, et al. Quantitative evaluation of tau PET tracers 18F-THK5351 and 18F-AV-1451 in Alzheimer's disease with standardized uptake value peak-alignment (SUVP) normalization. Eur J Nucl Med Mol Imaging. 2018;45:1596–604.
118. Endo H, Shimada H, Sahara N, et al. In vivo binding of a tau imaging probe, [11 C]PBB3, in patients with progressive supranuclear palsy. Mov Disord Off J Mov Disord Soc. 2019;34:744–54.
119. Gérard T, Colmant L, Malotaux V, et al. The spatial extent of tauopathy on [18F]MK-6240 tau PET shows stronger association with cognitive performances than the standard uptake value ratio in Alzheimer's disease. Eur J Nucl Med Mol Imaging. 2024;51:1662–74.
120. Kim M, Kim SJ, Park JE, et al. Combination of automated brain volumetry on MRI and quantitative tau deposition on THK-5351 PET to support diagnosis of Alzheimer's disease. Sci Rep. 2021;11:10343.
121. Leuzy A, Smith R, Ossenkoppele R, et al. Diagnostic Performance of RO948 F 18 Tau Positron Emission Tomography in the Differentiation of Alzheimer Disease From Other Neurodegenerative Disorders. JAMA Neurol. 2020;77:955–65.
122. Leuzy A, Pascoal TA, Strandberg O, et al. A multicenter comparison of [18F]flortaucipir, [18F]RO948, and [18F]MK6240 tau PET tracers to detect a common target ROI for differential diagnosis. Eur J Nucl Med Mol Imaging. 2021;48:2295–305.
123. Li L, Liu F-T, Li M, et al. Clinical Utility of 18 F-APN-1607 Tau PET Imaging in Patients with Progressive Supranuclear Palsy. Mov Disord Off J Mov Disord Soc. 2021;36:2314–23.
124. Liu F-T, Lu J-Y, Li X-Y, et al. 18 F-Florzolotau Positron Emission Tomography Imaging of Tau Pathology in the Living Brains of Patients with Corticobasal Syndrome. Mov Disord Off J Mov Disord Soc. 2023;38:579–88.
125. Messerschmidt K, Barthel H, Brendel M, et al. 18F-PI-2620 Tau PET Improves the Imaging Diagnosis of Progressive Supranuclear Palsy. J Nucl Med Off Publ Soc Nucl Med. 2022;63:1754–60.
126. Ossenkoppele R, Rabinovici GD, Smith R, et al. Discriminative Accuracy of [18F]flortaucipir Positron Emission Tomography for Alzheimer Disease vs Other Neurodegenerative Disorders. JAMA. 2018;320:1151–62.
127. Palleis C, Brendel M, Finze A, et al. Cortical [18 F]PI-2620 Binding Differentiates Corticobasal Syndrome Subtypes. Mov Disord Off J Mov Disord Soc. 2021;36:2104–15.
128. Schonhaut DR, McMillan CT, Spina S, et al. 18 F-flortaucipir tau positron emission tomography distinguishes established progressive supranuclear palsy from controls and Parkinson disease: A multicenter study. Ann Neurol. 2017;82:622–34.
129. Song M, Scheifele M, Barthel H, et al. Feasibility of short imaging protocols for [18F]PI-2620 tau-PET in progressive supranuclear palsy. Eur J Nucl Med Mol Imaging. 2021;48:3872–85.
130. Tagai K, Ono M, Kubota M, et al. High-Contrast In Vivo Imaging of Tau Pathologies in Alzheimer's and Non-Alzheimer's Disease Tauopathies. Neuron. 2021;109:42–e588.
131. Zou J, Park D, Johnson A, et al. Deep learning improves utility of tau PET in the study of Alzheimer's disease. Alzheimers Dement Amst Neth. 2021;13:e12264.

Figures

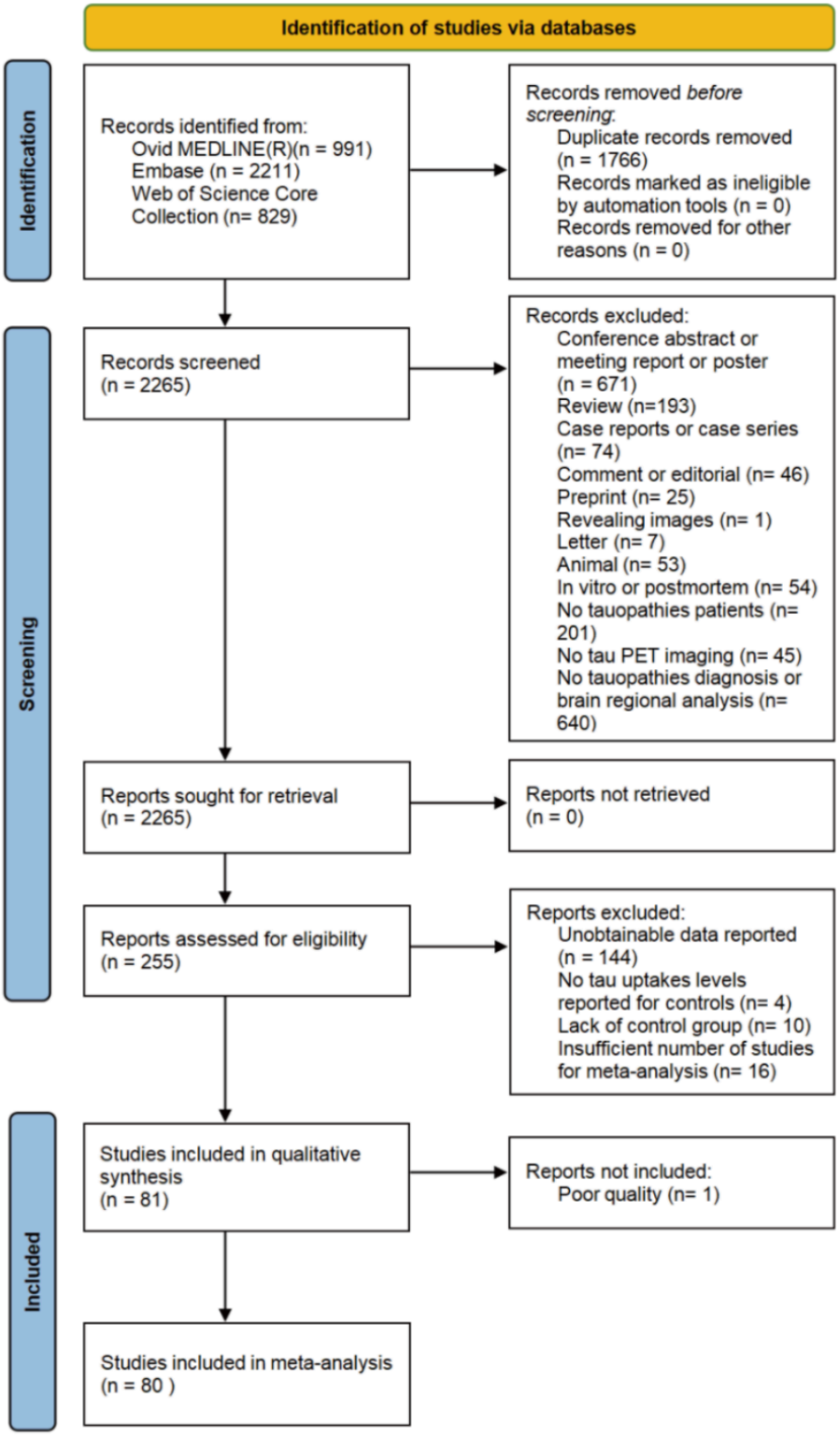


Figure 1

PRISMA (preferred reporting items for systematic reviews and meta-analyses) flow diagram of the search, screening, and inclusion process.

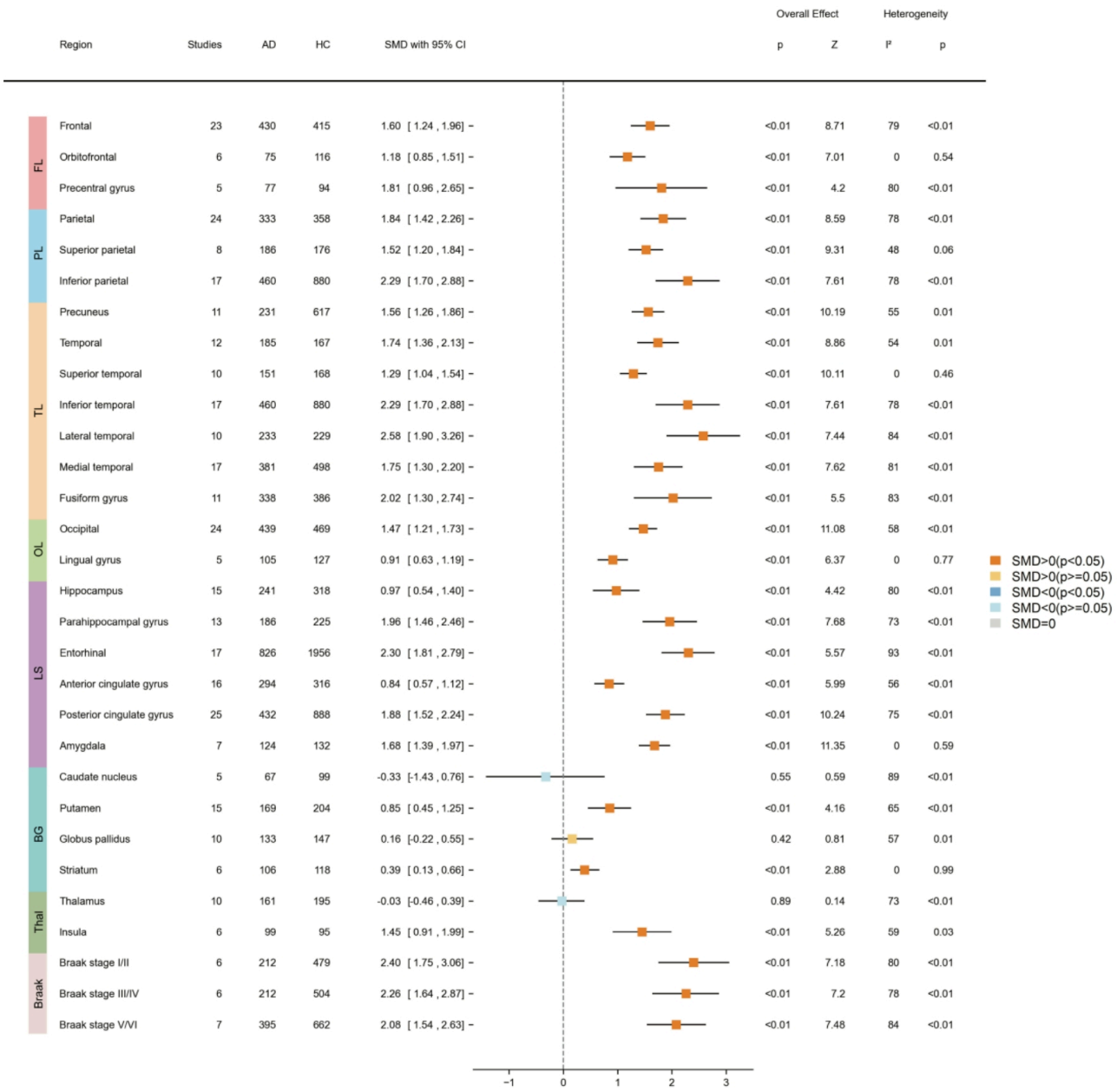


Figure 2

Results of the random effects meta-analysis of tau tracer uptake across different brain regions between patients with Alzheimer's disease and healthy controls.

The brain regions are presented according to their locations (FL, frontal lobe; PL, parietal lobe; TL, temporal lobe; OL, occipital lobe; LS, limbic system; BG, basal ganglia; and Thal, thalamus). The horizontal lines represent the 95% CIs of the SMD for each brain region. The color of the boxes signifies different interpretations: dark orange indicates SMD>0 and $p<0.05$; light orange indicates SMD>0 and $p\geq0.05$; dark blue indicates SMD<0 and $p<0.05$; and light blue indicates SMD<0 and $p\geq0.05$.

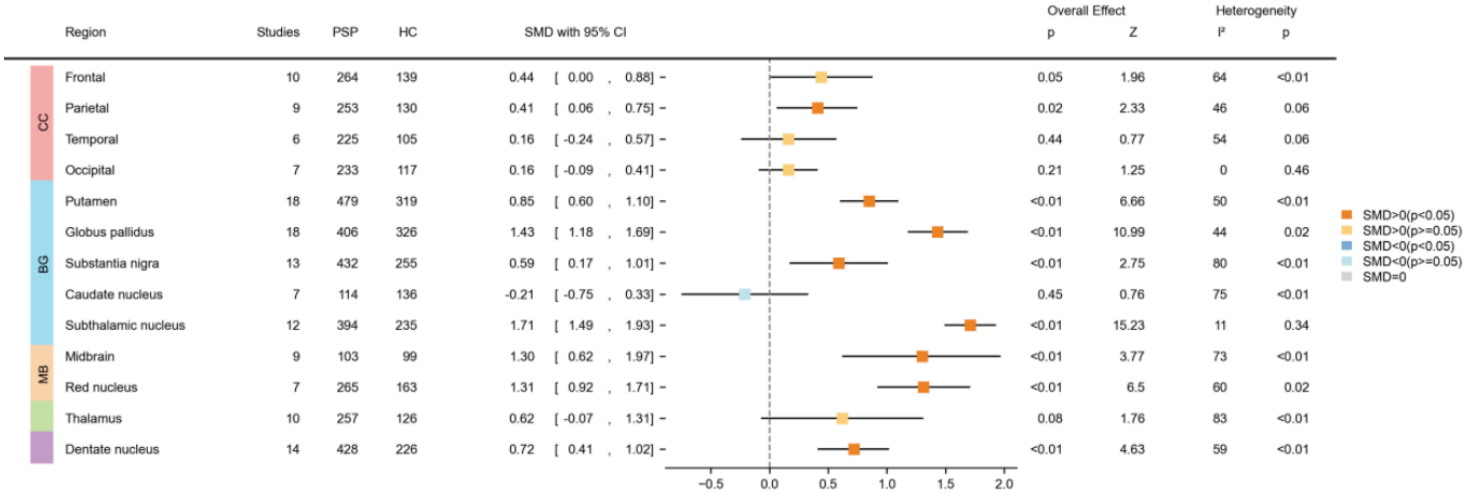


Figure 3

Results of the random effects meta-analysis of tau tracer uptake across different brain regions between progressive supranuclear palsy patients and healthy controls.

The brain regions are presented according to their locations (CC, cerebral cortex; BG, basal ganglia; MB, midbrain). The horizontal lines represent the 95% CIs of the SMD for each brain region. The color of the boxes signifies different interpretations: dark orange indicates SMD>0 and $p<0.05$; light orange indicates SMD>0 and $p\geq0.05$; dark blue indicates SMD<0 and $p<0.05$; and light blue indicates SMD<0 and $p\geq0.05$.

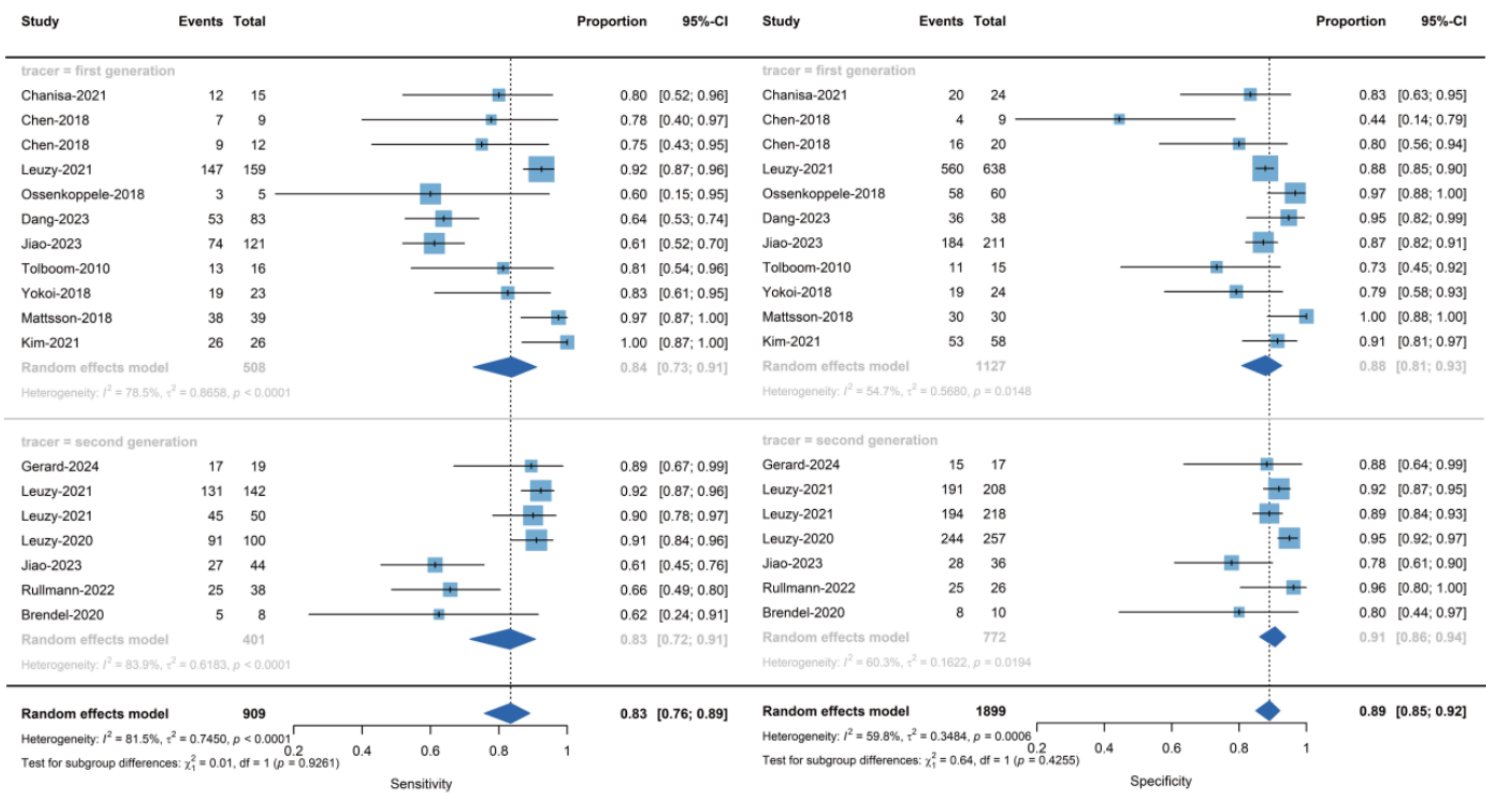


Figure 4

Forest plots illustrating the pooled sensitivity and specificity of tau PET for classifying patients with Alzheimer's disease and healthy controls.

The boxes represent point estimates proportional to the sample size of each study. Whiskers and the width of the diamonds indicate the 95% CIs for individual studies and the pooled random effects summary, respectively. The vertical dotted lines mark the pooled mean sensitivity and specificity for tau PET, while the diamonds illustrate the 95% CIs for the combined pooled mean. The total point estimate across all included tau PET studies is highlighted in bold black, whereas the aggregated values for the tau tracer generation setting subgroups are highlighted in bold gray. The *p* value for the comparison of subgroups was derived from a two-sided test for subgroup differences (random effects model).

Supplementary Files

This is a list of supplementary files associated with this preprint. Click to download.

- Supplementarytables.docx
- SupplementaryMethods.docx
- SupplementaryMaterial.xlsx
- SupplementaryFigure.docx